Phys Chem Minerals (2016) 43:237–265
DOI 10.1007/s00269-015-0790-5

ORIGINAL PAPER

Proton conduction and hydrogen diffusion in olivine: an attempt to reconcile laboratory and field observations and implications for the role of grain boundary diffusion in enhancing conductivity

Alan G. Jones[1,2]

Received: 25 March 2015 / Accepted: 7 December 2015 / Published online: 25 February 2016

Abstract Proton conduction in olivine is directly related to the diffusion rate of hydrogen by the Nernst–Einstein equation, but prior attempts to use this relationship have always invoked additional terms to try to reconcile laboratory measurements of proton conduction and hydrogen diffusion data. New diffusion experiments on olivine demonstrate that lattice diffusion associated with vacancies is indeed highly dependent on the defect site where hydrogen is bonded, but from none of the sites is diffusion fast enough to explain the observed laboratory proton conduction experiments. Hydrogen diffusion associated with polarons (redox-exchange) is significantly faster but still cannot explain the low activation energy typical of electrical conductivity measurements. A process of bulk diffusion, which combines lattice diffusion (either associated with redox-exchange or vacancies) with the far faster grain boundary diffusion, explains the laboratory results, but does not explain the field observations with an average grain size of 0.5–2 cm at 100 km below the Jagersfontein kimberlite field on the Kaapvaal craton. Either conduction is dominantly along well-interconnected grain boundaries of very fine-grained (0.01 mm) damp (80 wt ppm) olivine grains or fine-grained (0.05 mm), wet (400 wt ppm) pyroxene grains, or another conduction mechanism must be primarily responsible for the field observations. If diffusion is the correct explanation, the conductivity below the Gibeon kimberlite field in Namibia is too high to be explained by increased thermal state alone of a diffusion process, even for such fine-grained pyroxenes.

Keywords Electrical conductivity · Hydrogen diffusion · Grain boundary · Olivine · Pyroxene · Lithosphere

Introduction

It is only over the last 45 years that it has become appreciated that nominally anhydrous minerals (NAMs) can hold water, more correctly hydroxyl (OH), and consequently Earth's mantle is thought to be able to host an amount estimated to be at least that of the surface oceans, if not many times more, e.g., Beran and Zemann (1969), Fyfe (1970), Martin and Donnay (1972), Aines and Rossman (1984), Ahrens (1989), Bell and Rossman (1992), Hirschmann and Kohlstedt (2012a); see the recent excellent review by Demouchy and Bolfan-Casanova (2016). Mapping the presence and amount of this bound water in the mantle is crucial for understanding Earth's processes, as small amounts of water in NAMs affect both the physical and chemical behavior of the mantle; water significantly reduces viscosity and facilitates and promotes melting, chemical reactions, grain boundary migration, the development of certain crystallographic preferred orientations, and phase transitions (e.g., Bai and Kohlstedt 1992; Bell and Rossman 1992; Bolfan-Casanova 2005; Hirschmann and Kohlstedt 2012b; Hirth and Kohlstedt 1996; Jung and Karato 2001a, b; Karato 2006; Mei and Kohlstedt 2000a, b; Pommier 2014). Its presence controls the lithosphere–asthenosphere boundary (Green et al. 2010; Wang 2010)

Electronic supplementary material The online version of this article (doi:10.1007/s00269-015-0790-5) contains supplementary material, which is available to authorized users.

✉ Alan G. Jones
alan.jones.geophysics@gmail.com

[1] Dublin Institute for Advanced Studies, 5 Merrion Square, Dublin 2, Ireland

[2] Present Address: Complete MT Solutions, 5345 McLean Crescent, Manotick, Ottawa, ON K4M 1E3, Canada

is postulated to promote slip systems in olivine at asthenospheric conditions (Jung and Karato 2001a; Ohuchi et al. 2015), and differences in water content between the lower lithosphere and the asthenosphere likely account for the longevity of cratons (Katayama and Korenaga 2011; Peslier et al. 2010).

Direct petrological observation of water in situ is impossible; at best water content can be inferred petrologically from examination of mantle xenoliths (Bell and Rossman 1992) or mantle-derived magmas (Michael 1988), with an inherent time delay of many tens of millions of years. In addition, there are the issues of sampling bias and whether the water content measured in samples truly represents the ambient conditions (see discussion in Demouchy and Bolfan-Casanova 2016). Indirect real-time in situ observation is possible through using geophysical means, in particular using seismological and electromagnetic methods, albeit with spatially averaging resolution; these methods are discussed in the review paper by Karato (2006). Of these, the sensitivity of electromagnetic methods to lateral and vertical variations in electrical conductivity holds the greatest promise (Karato 2006).

The electrical conductivity of NAMs in silicate rocks at upper mantle conditions results from three mechanisms that sum to yield the bulk rock conductivity. These are (1) small polaron conduction, (2) proton conduction (by various species and from various sites in the lattice and on the grain boundaries), and (3) ionic conduction by magnesium vacancies. As is well known and I discuss and show below, at lithospheric pressure–temperature conditions and for interconnected pathways of grains less than around 1-mm proton conduction dominates over the other two by orders of magnitude, even for very low orders of water content (10 wt ppm); for larger grains then polaron conduction dominates at low temperatures and ion conduction at high temperatures. In contrast, seismic velocity requires a large amount of water to show measurable variation; it is affected by only 1 % for 1 wt% (10,000 wt ppm) water content, which far exceeds what is found above the transition zone by two orders of magnitude or more. Thus, determination of the electrical conductivity is the most attractive tool in the geoscientific arsenal for obtaining proxy estimations of the water content of NAMs in the upper mantle.

Unfortunately, the reported results from laboratories undertaking the electrical conductivity measurements on "wet" mantle minerals, particularly olivine, are in agreement neither with each other nor with field observations. This leads to directly contradictory inferences when one prefers to adopt the results of one laboratory over another. A prime example is the assertion of Yoshino et al. (2006) that hydrous olivine is unable to account for the conductivity anomaly at the top of the asthenosphere, a view that was contradicted by Wang et al. (2006) in the very same issue of *Nature* (see News and Views comment by Hirth 2006). Similarly, Huang et al. (2005) drew the conclusion that the transition zone is wet, but this view was contradicted by Yoshino et al. (2008) who concluded that it is dry. Based on Poe's water model (Poe et al. 2010), Naif et al. (2013) calculated that 800 wt ppm water is required for proton conduction to be the explanation of the observed asthenospheric conductivity below the Cocos Plate. As such high water content would invoke partial melting, the authors resolved that the more likely inference for the high conductivity observed was partial melt and concluded that they had observed a melt channel at the LAB. However, had the authors adopted Wang's water model instead (Wang et al. 2006), they would only have required 100–230 wt ppm water in olivine to obtain 4–6 Ωm at 1400 °C. These water content values are reasonable and bound the estimated amount of water carried by residual lherzolite in the mantle of 180 wt ppm (Green et al. 2010; corrected in Green et al. 2011), thus not requiring the invocation of partial melt. This is not to suggest that Wang's water model (Wang et al. 2006) is correct, although I do judge that it is correct for a given grain size as I will show below, but to demonstrate that choice of water model can lead to very different conclusions.

To make matters yet more complex, Jones et al. (2012) showed that none of the experimental data from the laboratories are consistent with well-calibrated, high-quality field observations for which bounded estimates of temperature, conductivity and water content exist. Also, not only do the different laboratories use different experimental techniques and different sample preparations, they also use different formalisms of the regression equation they employ to fit their laboratory data. However, it should be noted that none of the adopted equations is consistent with the Meyer–Neldel rule (MNR) that linearly relates the logarithm of the pre-exponent term to the activation energy term (Jones 2014b). Hydrogen diffusion in mantle minerals, especially olivine, was recently demonstrated to be consistent with the MNR (Jones 2014a); thus, proton conduction in those minerals must also be MNR consistent given the linear relationship between conduction and diffusion specified by the Nernst–Einstein equation.

Given these concerns related to the inconsistent experimental data on the electrical conductivity of wet olivine, I attempt to advance understanding of this issue through considering hydrogen diffusion in olivine in detail. Hydrogen diffusion and proton conduction are related through Nernst–Einstein equation, although attempts to apply this approach have met with varying success in the past, both in the geosciences and in solid-state physics. Ironically, in the solid-state physics literature, measurements are made of conduction in samples to determine diffusion rate, as conductivity is a simpler measurement to make than diffusion rate.

In this paper, I demonstrate that grain boundary diffusion dominates for the grain sizes used in multi-grain experiments in the laboratory and that the diffusion parameters measured by Demouchy (2010a; corrected in Demouchy 2012) fit the extrapolated experimental data of Wang et al. (2006) using their derived water model. However, I further demonstrate that effective diffusion in olivine, which combines lattice and grain boundary diffusion, and by inference in the other NAMs (pyroxenes), is insufficient to explain the high conductivity observed in the field for expected grain sizes of 0.5–20 mm, and either the dominant conduction is through well-interconnected networks of fine-grained (0.05 mm) pyroxenes, or another conduction mechanism has to be responsible.

Further review and discussion of this topic is given in Sect. 1 of the Supplementary Material.

FTIR spectra and water residence sites

Peaks in FTIR spectra identify the residence sites of H in olivine, and a full discussion of FTIR spectra and residence sites is given in Sect. 1.1 of the Supplementary Material. For our purposes, I refer to Berry et al. (2005) (cf. Fig. 1), who showed FTIR peaks in natural olivine at 3612 cm^{-1} for Si vacancy, 3572^{-1} and 3525 cm^{-1} for Ti-point defects, 3410 cm^{-1} for Ti planar defect, 3355^{-1} and 3325 cm^{-1} for Fe^{3+} defect, and 3160 cm^{-1} for Mg vacancy, and to Kovacs et al. (2010) with (Mg) peaks at 3220 and 3160 cm^{-1}, (Ti) peaks at 3572 and 3525 cm^{-1}, trivalent peaks between 3300 and 3400 cm^{-1}, and (Si) peaks at 3613, 3593, 3579, 3567, 3551, 3535, 3478, 3450, and 3405 cm^{-1}. Note that the Group I–H bands relate to (Ti) defects, the dominant and most prevalent incorporation mechanism (Berry et al. 2005; Schmadicke et al. 2013).

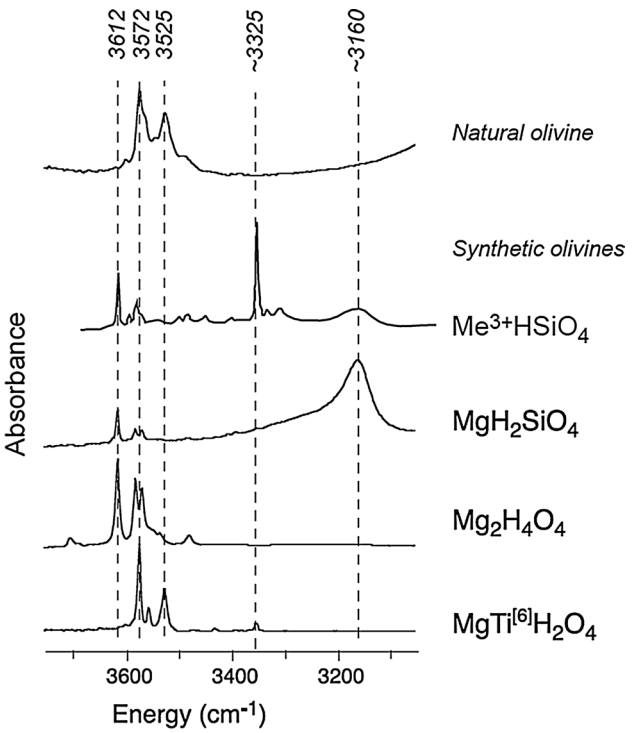

Fig. 1 Main four (point defect) substitution mechanisms in olivine showing the main spectral peaks at 3612, 3572, 3525, 3325, and 3160 cm^{-1}. Redrawn from Berry et al. (2007) and Walker et al. (2007)

Calibration of water in olivine

Determining the amount of "water" in a sample prior and subsequent to either diffusion or conduction experiments is absolutely crucial for ascertaining any water loss during the experiment. FTIR has been used in almost all experimental studies addressing the effect of water content on electrical conductivity, but not with consistent care. In principle, it is possible to accurately measure the water content if (1) the total absorbance (i.e., the sum of the absorbance along the three principal directions) and (2) the integral molar absorption coefficient, are both known. The source of errors is coming from these two values. A full review of this problem, especially as conducted by those measuring enhanced electrical conductivity in "wet" olivine, is given in Sect. 1.2 of the Supplementary Material. The reader is also referred to the synopsis in the recent review by Demouchy and Bolfan-Casanova (2016).

I recognize all of the issues detailed in that section related to IR spectra determination of the water content within the experimental samples. To be consistent throughout, I adopt the Bell calibration (Bell et al. 2003), and I correct the Paterson calibration water contents of Karato's group and Yoshino's group by a factor of 3.5 given their use of unpolarized FTIR spectra. This is slightly higher than the factor of 3 suggested by Ferot and Bolfan-Casanova (2012), but well within the combined 30 % error associated with IR spectra water estimates based on all of the various factors associated with the estimation (Demouchy and Bolfan-Casanova 2016).

The main point I wish to emphasize from these approximate water content corrections is that, with the sole exception of the single value of Yang (2012) at 40 wt ppm, all of the electrical conductivity laboratory experiments on olivine have been conducted at water contents far in excess of those found in the lithospheric mantle. As a consequence, the form of the regression equation adopted by the different laboratories to fit the experimental data becomes of paramount importance as that form dictates the nature of the extrapolation of the experimental data to lower water contents based on the fitted model values.

Maximum amount of water at lithospheric conditions

An important constraint on the maximum possible conductivity from proton conduction is the maximum possible water content bound in mantle minerals at lithospheric pressure–temperature conditions. Clearly proton conduction models that exceed that amount are untenable, a point exploited recently by Naif et al. (2013) in their argument that the high water contents derived from adopting the water model of Poe et al. (2010) were unjustifiable, hence inferring partial melt explained the high conductivities observed.

The water solubility in olivine is far less than the water storage capacity, and Bali et al. (2008) demonstrated for forsterite (Fo100) that water solubility is pressure and temperature dependent. Maximum values of 2000 wt ppm H_2O (Bell calibration) occur at 1250 °C, decreasing at lower and higher temperatures to ~500 ppm wt H_2O at 1000 and 1400 °C.

These values are all well in excess of the value of 180 wt ppm deduced by Green et al. (2010; corrected in 2011) for the total amount of water carried by residual lherzolite in the mantle. Kovacs et al. (2012) recently showed a significant drop in water storage capacity of peridotites at the vapor-saturated solidus, which is ~1025 °C at 2.5 GPa (75 km) and ~1200 °C at 4.0 GPa (120 km) (Green 1973), from 1000 to 190 wt ppm H_2O. Most recently, Green et al. (2014) demonstrated through their careful laboratory analyses that there can be high water contents up to 2000 wt ppm in the lithosphere at pressures less than 3 GPa (~100 km) in fertile mantle due to the presence of the hydrous mineral pargasite, but pargasite is unstable at greater pressures, and bulk water content drops to a maximum of 200 wt ppm.

More extensive discussion of this topic is given in Sect. 1.3 of the Supplementary Material.

Proton conduction in olivine

Conduction in olivine

There are three dominant conduction mechanisms in olivine in the mantle, and they combine serially through summing each charge carrier type to give the total conductivity, viz.

$$\sigma = \sigma_{sp} + \sigma_p + \sigma_i, \tag{1}$$

where σ is the total conductivity, σ_{sp} is small polaron hopping conduction, σ_p is proton conduction, and σ_i is magnesium vacancy ion conduction (Fullea et al. 2011; Pommier 2014; Yoshino and Katsura 2013; Yoshino et al. 2009a, b). These three are described by three Arrhenius equations, and the forms typically used are

$$\sigma = \sigma_{0sp}\exp\left(\frac{-\Delta H_{sp}}{kT}\right) + \sigma_{0sp}C_w^r\exp\left(\frac{-(\Delta H_p - \alpha C_w^{1/3})}{kT}\right) + \sigma_{0i}\exp\left(\frac{\Delta H_i}{kT}\right) \tag{2}$$

where all three have a pre-exponent term, σ_0, and an activation enthalpy (here just an activation energy, ΔH) term. The activation enthalpies, ΔH, are in eV, the water content, C_w, is in wt%, k is Boltzmann's constant, and the temperature, T, is in Kelvin.

Some authors include a pressure-dependent activation volume term to the activation enthalpy, i.e., $\Delta H + P\Delta V$ (e.g., Dai and Karato 2014b), and/or an oxygen fugacity term (fO_2) (e.g., Duba and Constable 1993), but those effects are second order compared with the dominant effects of proton conduction in the lithospheric mantle (although the experiments must be performed under controlled fO_2, as demonstrated initially by Duba and Nicholls (1973) and Duba (1976), and confirmed by many authors since).

Small polaron conduction and ionic conduction contributions

Small polaron conduction is enabled by electron holes hopping between ferrous (Fe^{2+}) and ferric (Fe^{3+}) iron and is the dominant conduction process in dry olivine at shallow to middle lithospheric temperatures (<1000 °C). Ionic conduction dominates at higher temperatures (>1250 °C) as a consequence of the creation of cation magnesium vacancies $\left(V''_{Mg}\right)$. The physics of these two processes is described in detail in the review paper of Yoshino (2010). Although this paper focuses on proton conduction enabled through hydrogen diffusion, a complete treatment of the contributions to electrical conductivity from small polaron conduction and ionic conduction is discussed in Sect. 2.1.1 in the Supplementary Material.

Figure 2 shows a plot of small polaron conduction (thin black line labeled J2009) and magnesium vacancy conduction (thin blue line labeled F2011), and both summed together (thick red line), for dry olivine with Mg# = 92.0 in the temperature range of the coldest cratonic mantle to the transition zone (400–1500 °C, where temperatures beyond the lithosphere-asthenosphere boundary, taken here as 1350 °C, are indicated by the purple hatched field). For this paper, I am concerned with conductivity between 740 °C and 850 °C so I only need to consider small polaron conduction, σ_{0sp}, and not magnesium vacancy conduction.

Proton conduction

In the case of proton conduction, σ_{0p}, there are water-dependent terms (functions of C_w) added to both the pre-exponent term and the activation energy term in the

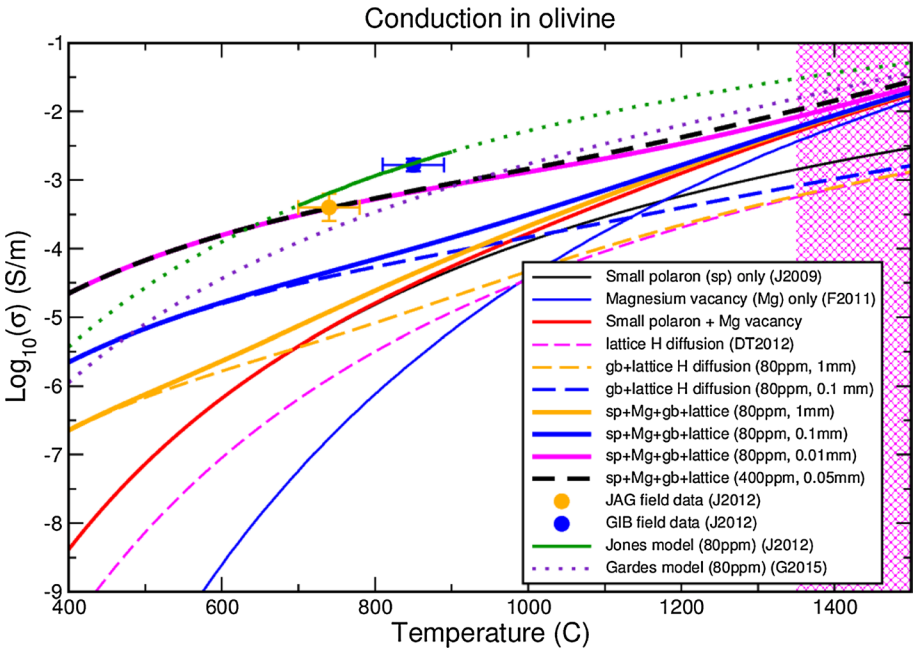

Fig. 2 Conduction in olivine with temperature. Small polaron conduction (J2009, *thin black line*, from Jones et al. (2009)) and magnesium vacancy conduction (F2011, *thin blue line*, from Fullea et al. (2011)) in dry olivine, and their sum (*thick red line*). Conduction model of Jones et al. (2012) (J2012, *thick green line*, *solid* in the temperature range of 700–900 °C, and *dotted* outside that range where the model is extrapolated) for 80 wt ppm. Total conductivity summing all three processes for the recent model of Gardes et al. (2015) (G2015, *thick dotted purple line*). Conductivity from effective diffusion derived for 80 wt ppm water using the Nernst–Einstein equation and the grain boundary diffusion data from Demouchy (2010a) and lattice diffusion data from Du Frane and Tyburczy (2012) shown for 10 mm (*dashed orange line*) and 3 mm (*dashed blue line*). Total conductivity, summing the effects of small polaron conduction (insignificant), magnesium vacancy ion conduction (important at temperatures in excess of 1300 °C, i.e., base of the lithosphere/top of the asthenosphere), and proton conduction from grain boundary diffusion (plus lattice diffusion, but that is insignificant) for 80 wt ppm water shown as *solid orange* (10 mm grain size) and *solid blue* (3 mm grain size) lines. Total conductivity with a water content of 200 wt ppm for grain size of 10 mm shown as *dashed-dotted orange line*. The JAG (*orange filled circle with error bars*) and GIB (*blue filled square with error bars*) field data come from the Jagersfontein (Kaapvaal Craton) and Gibeon (Rehoboth terrane) kimberlite fields, respectively (see Jones et al. 2012). The *purple* hatched region indicates the asthenosphere (assumed to be at a temperature >1350 °C)

generalized form represented in Eq. (2). The notion that the fast rates of hydrogen diffusion could lead to significant charge carrying effects that would enhance conduction in the mantle was first proposed by Karato (1990), in what has become a landmark and highly influential paper. Experimental support for this suggestion by Karato did not come for another 15 years. During the past decade, various laboratories have been undertaking the difficult measurements to derive proton conduction in olivine as a function of temperature and water content, and they use different formalisms to fit their laboratory observations. Karato's and Wang's (Dai and Karato 2009; Huang et al. 2005; Wang et al. 2006, 2008) laboratories and others (Yang et al. 2011, 2012) use a non-unity value of r and a zero value for α, whereas the laboratories of Yoshino (Yoshino and Katsura 2012; Yoshino et al. 2009a, b) and Poe (Manthilake et al. 2009; Poe et al. 2010) set r to unity and determine a nonzero positive value for α. (Note that the Wang et al. (2008) formalism also includes an iron-dependent term and a pressure term that are ignored here as the effects of both are second order compared with the water content effect.)

The exponent r on the pre-exponent water content C_w in Karato's and Wang's formalism is an attempt to describe nonlinear effects due to multiple hydrogen atoms in a single defect, but is ignored by Yoshino and Poe who set $r = 1$. Note that plastic deformation of olivine due to water content also includes an exponent term r on the water content for both diffusion and dislocation creep (Chu and Korenaga 2012; Mei and Kohlstedt 2000a, b).

In contrast, the coefficient α used by Yoshino and Poe is an attempt to describe activation energy dependence as a function of water content that results from more closely spaced defects, but is ignored by Karato and Wang who set $\alpha = 0$. Water content C_w in this activation enthalpy term is taken to the power 1/3 following the standard solid-state physics equation for an n-type semiconductor (Yoshino and Katsura 2013). Poe et al. (2010) applied both formalisms and adopted the Yoshino one based on goodness of fit of the models to the data. Recently, Gardes et al. (2015) fit

all available laboratory data, without discrimination, using both formalisms and also concluded, based on obtaining a superior fit, that the Yoshino/Poe formalism is best. However, in order to address the issue of the bias of water content estimates that had been derived using unpolarized FTIR spectra with Paterson calibration, Gardes et al. (2015) expanded the errors of those estimates to encompass both the random errors and the bias errors, i.e., they expanded the upper bounds of the errors by a factor of 4. With such wide errors, it is hardly surprising that the authors were able to find compatible solutions to almost all of the laboratory data.

Again it must be highlighted that almost all of the laboratory experiments were conducted with water contents in olivine far in excess of what is observed and permissible in the lithosphere, i.e., approximately 200 wt ppm bulk water (see Table 1 and Fig. 3b). Thus, the formalism adopted dictates how the laboratory data are extrapolated from high laboratory water contents to lower lithospheric water contents. As such, adopting one formalism over another for a model of water content in the lithospheric mantle based solely on goodness of fit is highly questionable.

Jones et al. (2012) adopted both of these terms (r and α) in their model fitting of field data, but the limited range of C_w in the field data (assumed to vary between 60 and 100 wt ppm, whereas laboratory data are often measured at water contents of hundreds of wt ppm) meant that estimates of both r and α had large errors associated with them.

Jones (2014b) discussed these two formalisms in detail, based on the proton conduction term in Eq. (2), and showed that neither of them is consistent with the Meyer–Neldel rule (called the Compensation Law in chemistry) by which the logarithm of the pre-exponent term and activation enthalpy terms are linearly related. Hydrogen diffusion in olivine has been demonstrated to be consistent with the MNR (Jones 2014a), thus inferring that proton conduction also should be consistent with the MNR through the linear Nernst–Einstein relationship (see below).

Laboratory conductivity measurements of proton conduction in olivine

As discussed above, determination of the electrical conductivity due to proton conduction in olivine has only been undertaken within the last decade. A brief comparison of the laboratory experiments is given in Table 1, together with the models fit to the experimental data adopting the proton conduction term in Eq. (2). Of note is that none of the experimentalists used the same type of sample preparation, nor the same temperature ranges, nor the same pressure ranges, nor the same water contents, nor the same frequency measurements, nor the same water calibration. This lack of consistent application of laboratory technique makes inter-comparison of the experiments difficult to impossible.

Table 2 lists the laboratory data of conductivity with varying water content at 740 °C. Data from Wang et al. (2006) were calculated to 740 °C with an assumed value of activation energy of 3.00 (see Jones et al. 2012). All others were obtained from extrapolating or interpolating the plotted curves in the respective publications or from applying the published water models. All data are plotted in Fig. 3, where in the case of Paterson calibration the original data are shown as open symbols and Bell calibration corrected data (see Sect. 2.2, Supplementary Material) as filled symbols.

The lines on Fig. 3 are the water models published by the various authors (see Table 2), where the water models of Wang et al. (2006) (black lines) and Yoshino et al. (2009) (red lines) have been multiplied by 3.5 to "correct," to first order, to Bell calibration. The solid parts of the lines indicate the water content ranges of the experiments, and the dashed parts indicate extrapolations to zero water content (and in some cases to higher water content). Note that, as highlighted in Fig. 3b, with the sole exception of Yang (2012), none of the other experiments had water contents in the samples that simulated those found in the lithospheric mantle (typically <150 wt ppm). Thus, the extrapolations to lithospheric water contents are entirely dictated by the form of the regression equation adopted to fit the laboratory data at higher water contents.

Also plotted on Fig. 3 is the water model from the attempt by Gardes et al. (2015) to reconcile the disparate laboratory observations. The full Gardes et al. (2015) model, including the effects of small polaron, magnesium vacancies, and proton conduction, for a temperature of 740 °C is shown in Fig. 2 (labeled G2015, *dotted purple line*) and Fig. 3 (labeled G2015, *blue dashed line*). However, again the extrapolated shape of the model for realistic lithospheric water contents (i.e., <200 wt ppm) is entirely dictated by the form of the equation used to fit the data (see Fig. 3b). Note that the model comes reasonably close to the JAG and GIB field data values, to within half an order of magnitude, but does not fit them (Fig. 2).

Further discussion of laboratory conductivity measurements of proton conduction in olivine, particularly the Gardes et al. (2015) work, is given in Sect. 2.2 of the Supplementary Material.

Criticisms of laboratory work

Those who conduct electrical conductivity studies of olivine in the laboratory are strongly arguing in the literature in defense of their own results and in opposition of those of others. Particularly, Karato and Yoshino have exchanged a number of criticisms of each other's work related to sample

Table 1 Details of laboratory experiments to determine proton conduction in olivine with the derived Arrhenius model used to fit the laboratory observations

Reference	Sample description	Mg#	T (C)	P (GPa)	Cw range (wt ppm) Calibration	FTIR spectra	Pre-exponent $\log_{10}(\sigma_0)$ *r*	Activation energy ΔH (eV) α	Comments	$\log_{10}(\sigma)$ @ 740 °C for 80 wt ppm (proton conduction only)
Wang et al. (2006)	Hot-pressed olivine aggregates Grain size 10–30 μm		600–1000	4	100–800 Paterson	Does not say whether polarized or unpolarized. Inspection of spectra suggests unpolarised 3,400 cm^{-1} broad peak 3,500 and 3,600 cm^{-1} sharp peaks	3.0 ± 0.2 0.62 ± 0.15	0.87 ± 0.05 *0*	Corrected FTIR spectra for broad "grain boundary peak" at ~3,410 cm^{-1}	−2.63 (−2.97[a])
Yoshino et al. (2006)	Single crystal 10×10×14 mm	92	223–1227	3	5–218 Paterson	Unpolarized FTIR FTIR spectra used, but no discussion of peaks	0.37 *1*	0.73 *0*	[100]	−3.26 (No water content term)
							0.87 *1*	0.93 *0*	[010] significant dehydration	Not reliable
							0.88 *1*	0.87 *0*	[001] significant dehydration	Not reliable
Wang et al. (2008)[1]	Dunite Grain size 0.5–1.5 mm		1000–1300	2–3	Bulk rock 22 Paterson	No FTIR shown	5.2 ± 0.4 0.67 ± 0.07	1.90 ± 0.09 *0* +Xfe[b](0.82 ± 0.03)	FTIR after expt., not before, so do not know water loss Done at high temps above 1000 K, so must have had water loss—but it is a very low value Dunite—not olivine	−5.61 (−6.02[a])
Yoshino et al. (2009a, b)	<1 μm powder pressed	92.5	727–1227	10	400–2900 Paterson	Unpolarized FTIR Two strong absorption bands at 3567 and 3611 cm^{-1} Spectra before and after very similar	1.9 ± 0.44 *1*	0.92 ± 0.04 0.16 ± 0.02	Single-frequency (0.1 Hz) measurements Bell et al. (2003) suggest need to multiply Cw from unpolarised FTIR by 3.5	−4.61 (−5.55[a])

Table 1 continued

Reference	Sample description	Mg#	T (C)	P (GPa)	Cw range (wt ppm) Calibration	FTIR spectra	Pre-exponent $\log_{10}(\sigma_0)$ *r*	Activation energy ΔH (eV) α	Comments	$\log_{10}(\sigma)$ @ 740 °C for 80 wt ppm (proton conduction only)
Poe et al. (2010)[2]	Single crystal SCO 1.8 mm dia. × 2 mm	90	850–1436	8	363–2215 Bell	"We observe several strong absorption bands at lower OH stretching frequencies (3300–3500 cm^{-1}) in our synthetically hydrated samples which do not appear in the spectra of natu ral olivine samples having much lower H2O concentrations"	2.59 ± 0.16 *1* 3.46 ± 0.09 *1* 1.02 ± 0.09 *1*	1.26 ± 0.04 1.18 ± 0.04 1.50 ± 0.05 1.43 ± 0.11 0.812 ± 0.016 0.70 ± 0.015	[100] [010] [001]	−4.60 −4.68 −4.42
Yang (2012)	Single crystal		200–800	1	40 Bell	Polarized FTIR	0.93 ± 0.26 No Cw term	0.95 ± 0.04 *0*	Crust–mantle conditions Why so conduct-ing? Is single crystal so should be same as conductivity from diffu sion on single crystal	N/A
Dai and Karato (2014c)	SCO power <5 μm annealed at P = 4 GPa and T = 1473 K for 3 h	NR	600–1000	4	280 Paterson	Unpolarized FTIR before and after	Re-ReO_2 1.67 ± 0.08 0.62 Ni–NiO 2.00 ± 0.13 0.62 Mo–MoO_2 1.69 ± 0.10 0.62	Re-ReO_2 0.88 ± 0.05 *0* Ni–NiO 0.91 ± 0.03 *0* Mo–MoO_2 0.81 ± 0.04 *0*	*r* fixed from Wang et al. [Wang et al. 2006]. Also included an oxygen fugac-ity term in the pre-exponent component	N/A

Table 1 continued

Reference	Sample description	Mg#	T (C)	P (GPa)	Cw range (wt ppm) Calibration	FTIR spectra	Pre-exponent $\log_{10}(\sigma_0)$ r	Activation energy ΔH (eV) α	Comments	$\log_{10}(\sigma)$ @ 740 °C for 80 wt ppm (proton conduction only)
Dai and Karato (2014b)	SCO power <5 μm annealed at P = 4 GPa and T = 1473 K for 3 h	NR	600–1000	4–10	160 Paterson	Unpolarized FTIR before and after	2.28 + 0.02/−0.03 [a](1-BP) where P = pressure (GPa), B = 0.028 ± 0.003	0.95 ± 0.04 *0* +PV/RT where P = pressure (GPa), V = −0.85 ± 0.05	Data fit to an equation that includes pressure-dependent pre-exponent and activation energy terms	N/A
Dai and Karato (2014a)	SCO single crystal Disk-shaped 1.6 mm dia. 0.4 mm thick	NR	300–1100	4	460 Paterson		1: 0.74 ± 0.09 2: 4.52 ± 0.20	1: 0.78 ± 0.02 2: 1.45 ± 0.06	[100]	Two conduction mechanisms, (1) a low temperature one and (2) a high temperature one
							1: 0.51 ± 0.04 2: 1.99 ± 0.16	1: 0.76 ± 0.02 2: 1.05 ± 0.03	[010]	
							1: 0.30 ± 0.10 2: 1.08 ± 0.13	1: 0.73 ± 0.02 2: 0.90 ± 0.05	[001]	

Where a model has been proposed based on multiple water contents, the predicted conductivity at 740 °C is listed in the rightmost column. NR: Not reported. N/A: Not applicable. Water contents (wt ppm H_2O) and calibration approach used listed in column 6

Italicized values infer implicitly assumed

The Arrhenius model values of Poe et al. (2010, their Table 3) have been converted from wt ppm water to wt%. For σ_0 this means multiplying by 10^4 then taking the base-10 logarithm. For α this means multiplying by 21.54 (i.e., $(10^4)^{1/3}$)

[a] Calculation for water content of 22.6, which is 80/3.5 to correct Paterson calibration to Bell calibration

[b] Wang et al. (2008) include an iron content term (Xfe) in the activation energy, which, for typical olivine Mg#'s observed in the lithosphere, reduces the activation energy by an amount of the same order as the error in its determination (0.08). NR: not reported. N/A: not applicable

preparation, laboratory procedures, sensitivity of the sensing equipment, conductivity measurements, pressure conditions, oxygen fugacity conditions, water content evaluation, etc. (Dai and Karato 2014b; Karato 2011; Karato and Dai 2009; Karato and Wang 2013; Yoshino 2010; Yoshino and Katsura 2009, 2013; Yoshino et al. 2008, Supplementary Information). Yang (2012) is highly critical of prior experiments, citing a number of issues particularly in the work of Yoshino et al. (2006) and of Poe et al. (2010), and Karato (2015) discusses the anomalous nature of the results of Poe et al. (2010). A full review of the problems with prior experiments is given in Sect. 2.2.1 of the Supplementary Material. In conclusion, none of the laboratory experiments reported to date are without significant and substantial criticism and all must be viewed with caution. These differences attest to the complexity and difficulty in performing these experiments and the exquisite care and attention to detail that is required for all steps. It is though certainly not the case that the average of all of these experiments, as performed by Gardes et al. (2015), has any meaning.

FTIR spectra of published results

Given the observations above that FTIR spectra can indicate the water residence sites, we can examine the published FTIR spectra of those who undertook conductivity measurements to deduce the likely conductive process.

The FTIR spectra in Wang et al. (2006, Supplementary Information 2) is dominated by peaks at 3400 and 3500–3600 cm^{-1}, indicative of hydrogen predominantly in Si-vacancies, plus grain boundary effects that are ignored; the lines associated with trivalent and Mg-vacancies are very minor to absent. As I will show below, given the very low diffusion rate for Si-vacancies the high conductivity observed cannot due to the process of diffusion from the dominant hydrogen site identified by the spectra, but must be associated with diffusion at the higher spectral band with far lower amplitude indicative of grain boundary diffusion.

Neither Yoshino et al. (2006) nor Wang et al. (2008) provide plots of their FTIR spectra.

In Yoshino et al. (2009a, b), the spectra are dominated by hydrogen in Si-vacancies (the spectra are too noisy to see the proportion of trivalent and Mg-vacancies, but they seem to be very minor), the slowest diffusion process. The peak observed after the conductivity measurements at 3400 cm^{-1} in their Fig. 2a is quite strange. The position corresponds to titanoclinohumite lamellae (i.e., a hydrous phase where the OH is structurally bounded, like in amphiboles). Another interesting feature is the presence of fluid inclusions producing a broad band centered around 3400 cm^{-1} (this is referred in the paper as a higher background).

In Poe et al. (2010), the spectra are dominated by hydrogen in Si-vacancies but with a significant proportion of trivalent peaks (most probably $Fe3^{+}$, doublet at around 3325 and 3355 cm^{-1}).

The spectra in Yang (2012) are interesting. It is dominated by Ti-point defects, and trivalent and Mg-vacancies. Except for the H in Mg-vacancies (not very common), these spectra are probably what we expect to see for lithospheric olivines.

The spectra in Dai and Karato (2014b) and Dai and Karato (2014c) only infer Si-vacancies, a slow diffusing mechanism. Their observed conductivities cannot be explained by H diffusion from these sites. The FTIR spectra of Dai and Karato (2014a) (Figures S-4 and S-5 in their Supplementary Material) are dominated by two sharp peaks at approximately 3570 and 3640 cm^{-1}, indicative of Ti-point defects and Si-vacancies, respectively, which are the two slowest diffusing mechanisms, by orders of magnitude, and cannot explain the observations.

Laboratory diffusion measurements

There are two basic classifications of diffusion that occur both in the Earth and in experimental studies: volume diffusion that relates to diffusion within the interior of a phase (be it a mineral or a melt) and boundary diffusion that relates to diffusion on the boundary of two phases. These are not exclusive processes; as described by Balluffi et al. (2005) atoms can diffuse partly within the grains and partly on the grain boundaries. Watson and Baxter (2007) describe diffusion generally in an informative, educational review for the non-expert.

A comprehensive overview of diffusion in minerals and melts is given in Zhang (2010) from the Reviews in Mineralogy and Geochemistry Volume 72 on Diffusion in Minerals and Melts (Zhang and Cherniak 2010). The chapter by Farver (2010) gives an first-rate overview review of diffusion by H and O in minerals, and the chapter by Brady and Cherniak (2010) discusses diffusion by various species (O, Sr, Ca, Mg, Pb, H, Si, and Ar) in minerals; both contain highly useful databases that were exploited by Jones (2014a). The chapter by Chakraborty (2010) discusses diffusion coefficients for various species (Fe–Mg, Si, O, Ca, Ni, H, Sr) in olivine and its high-pressure metamorphs, demonstrating that H diffusion is faster than any other species by many orders of magnitude. Demouchy and Bolfan-Casanova (2016) give a recent review of hydrogen diffusion in NAMs.

Table 3 lists high-quality, robust experimental observations of diffusion in olivine initiating with those of Mackwell and Kohlstedt (1990) 25 years ago to the most recent reported by Padrón-Navarta et al. (2014). A more extensive listing of all experiments and model calculations found in the literature is given in the Supplementary

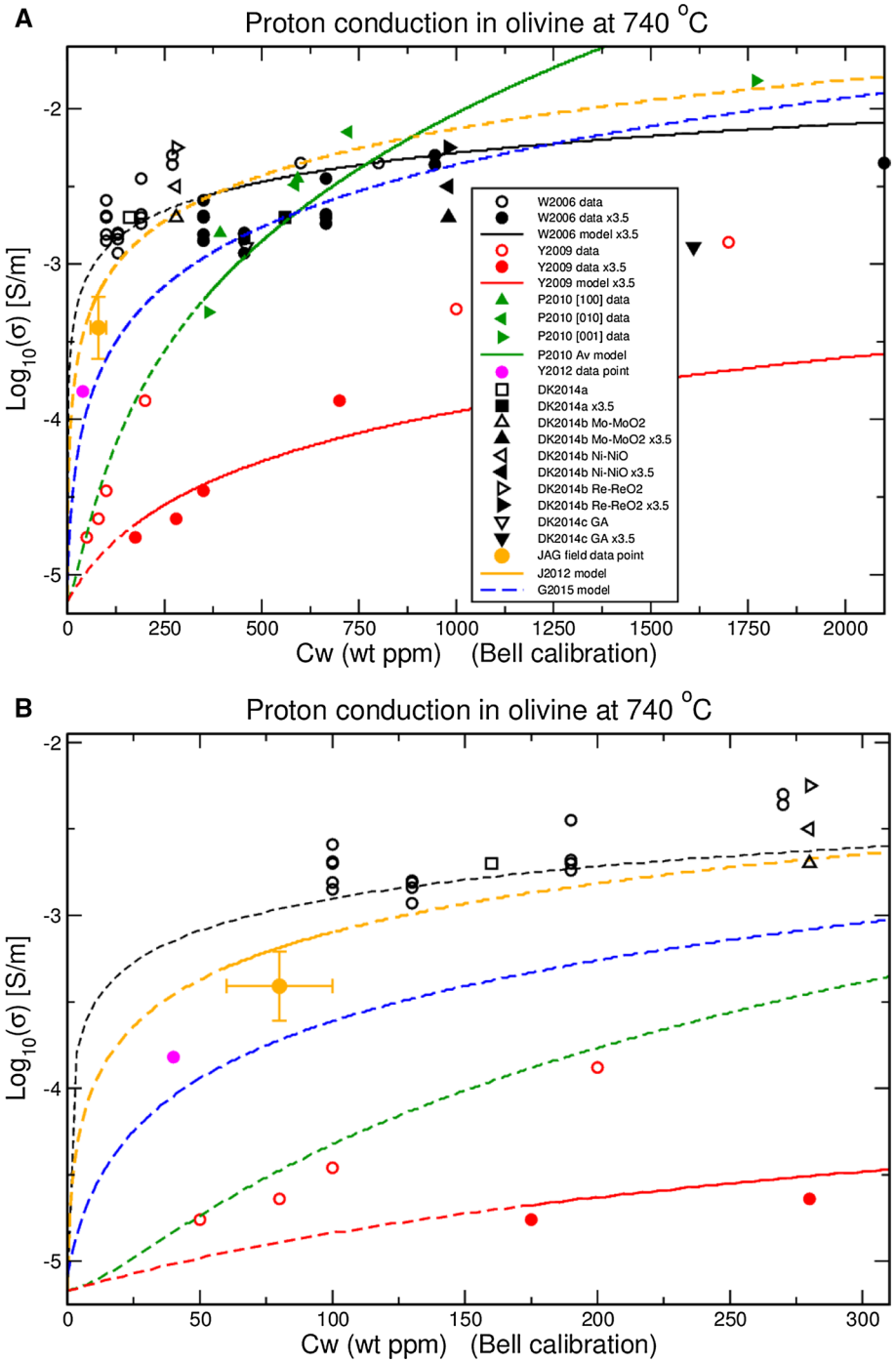

Fig. 3 Laboratory data of conductivity with varying water content at 740 °C in the range of **a** 0–2000 wt ppm and **b** 0–300 wt ppm. Data from Wang et al. (2006) calculated to 740 °C with an assumed value of activation energy of 3.00. All others obtained from the plotted curves in the respective publications through interpolation or extrapolation. Karato's laboratory—data derived from publications as *open black symbols*, Bell calibration corrected (×3.5) as *filled black symbols*; circles from Wang et al. (2006) (W2006), *squares* from Dai and Karato (2014b) (DK2014a), *up*, *left*, and *right triangles* from Dai and Karato (2014c) (DK2014b), *down triangles* from Dai and Karato (2014a) (DK2014c). Yoshino's laboratory—derived from publication as open red circles, Bell calibration corrected (×3.5) as *filled red circles* (Yoshino et al. 2009a, b); Poe's laboratory—derived from publication as *green triangles* (Poe et al. 2010) (P2010); Yang's laboratory—derived from publication as *purple circle* (Yang 2012) (Y2012). Also plotted are the regression water models reported by the various authors, where the water models of Wang et al. (2006) (W2006 model) and Yoshino et al. (2009a, b) (Y2009 model) are corrected to Bell calibration by multiplying by 3.5. *Solid lines* indicate the regression models where experimental data exist, and *dashed lines* where the models are extrapolated by the formulae used to fit the laboratory observations. Also plotted are the field data point at 100 km below the Jagersfontein kimberlite field (*orange circle* with *error bars*), and the model derived to fit that data point plus one from the Gibeon kimberlite field on the Rehoboth terrane, Namibia (Jones et al. 2012), *solid orange line* where constrained by the water content and *dashed orange line* where extrapolated by the regression formula adopted

Table 2 Laboratory data of conductivity with varying water content at 740 °C

References	Water content (ppm)	σ (S/m)	Temperature (°C)	Log_{10}[σ (S/m)] at 740 °C	Comments Sample/run number, other comments
Wang et al. (2006) Corrected to Bell calibration for water content[1]	270 → 945	0.0025	687	−2.36	K428
	270 → 945	0.0386	1000	−2.30	K428
	800 → 2800	0.0010	608	−2.35	K462
	600 → 2100	0.0009	600	−2.35	K468
	190 → 665	0.0273	1000	−2.45	K488
	190 → 665	0.0032	800	−2.74	K488
	190 → 665	0.0014	700	−2.68	K488
	190 → 665	0.0004	600	−2.70	K488
	130 → 455	0.0133	1013	−2.80	K492
	130 → 455	0.0055	898	−2.84	K492
	130 → 455	0.0026	795	−2.81	K492
	130 → 455	0.0007	690	−2.93	K492
	100 → 350	0.0108	1000	−2.85	K500
	100 → 350	0.0060	900	−2.81	K500
	100 → 350	0.0036	800	−2.69	K500
	100 → 350	0.0017	700	−2.59	K500
	100 → 350	0.0004	600	−2.70	K500
Yoshino et al. (2009a, b) corrected to bell calibration for water content[1]	50 → 175			−4.76	
	80 → 280			−4.64	
	100 → 350			−4.46	
	200 → 700			−3.88	
	1000 → 3500			−3.29	
	1700 → 5950			−2.86	
Poe et al. (2010)	383			−2.80	[100]
	592			−2.45	
	1903			−0.80	
	585			−2.49	[010]
	722			−2.15	
	363			−3.31	[001]
	1771			−1.82	
	2215			−1.57	
Du Frane and Tyburczy (2012)	100			−5.6	Based on diffusion calculation
Yang (2012)	40			−3.82	Measurements made on all three axes, but gave same result
Dai and Karato (2014c) corrected to Bell calibration for water content[1]	280 → 980			−2.7	K1403, Re–ReO_2
				−2.5	K1398, Ni–NiO
				−2.25	K1400, Mo–MoO_2
Dai and Karato (2014b) corrected to Bell calibration for water content[1]	160 → 560			−2.7	K1318, K1321, K1323
Dai and Karato (2014a) corrected to Bell calibration for water content[1]	460 → 1610			−2.6 (m)	[100]
				−2.9 (m)	[010]
				−3.1 (m)	[001]
				−2.9 (m)	Geometrical average of series and parallel conductivities

Data from Wang et al. (2006) calculated to 740 °C with an assumed value of activation energy of 3.00. All others obtained from the plotted curves in the respective publications or from the model fit parameters (m). All data plotted in Fig. 3

Correction made for unpolarized Paterson calibration to Bell calibration by multiplying water contents by 3.5

Table 3 Details of laboratory experiments to determine hydrogen diffusion in olivine with the derived Arrhenius model used to fit the laboratory observations and predicted conductivity using Nernst–Einstein equation for 80 wt ppm at 740 °C

	Sample description	Type of experiment	Mg#	T (C)	P (GPa)	Cw range (wt ppm) Calibration	FTIR spectra	Pre-exponent $\log_{10}(D_0)$ (m^2/s)	Activation energy (kJ/mol)	Comments	$\log_{10}(\sigma)$ @ 740 °C for 80 wt ppm
Mackwell and Kohlstedt (1990)	SCO	H uptake	91	800–1000	0.3	2–10 Paterson	Unpolarized	−4.22 +0.17/−0.30	130 ± 30	[100]	−5.10
								−5.30 +0.25/−0.70	130 ± 30	[001] assumed same ΔH as [100] so is suspect D_0 value	−5.72
Kohlstedt and Mackwell (1998)	SCO	H uptake	91	800–1000	0.2	2 Paterson	Polarized	−3.85	145 ± 30	[100]	−5.04
								−3.82	180 ± 50	[010]	−6.82
								−6.83	110 ± 50	[001]	−6.22
						10 Paterson		2.01[a]	260 ± 20	[100]	−5.11
								0.97[a]	260 ± 20	[010]	−6.15
								1.60[a]	260 ± 20	[001]	−5.52
Demouchy and Mackwell (2003)	Pure Forsterite Mg_2SiO_4	H uptake	100	900–1100	0.2 and 1.5	2–6 Paterson	Polarized	−3.3 ± 1.3	210 ± 33	[001]	−7.84
								−4.1 ± 1.2	205 ± 31	[010]	−8.39
								−3.8 ± 1.6	225 ± 40	[100]	−9.12
Demouchy and Mackwell (2006)	SCO	H uptake	90	900–1000	0.2 and 1.5	10–20 Paterson	Polarized	−4.5 ± 4.1	204 ± 94	[100] and [010] analyzed together	−8.74
								−1.4 ± 0.5	258 ± 11	[001]	−8.42
Demouchy (2010a); Demouchy (2012)	SCO	H uptake	91	1000–1200	0.3	2–10 Paterson	Unpolarized	−6.2 ± 0.1	71 ± 10	Effective diffusion	−3.58
								−3.4 ± 0.1	54[1] ± 4	Grain boundary diffusion	0.098
Du Frane and Tyburczy (2012)	Single crystals SCO	Isotope inter-diffusion	89	750–900	2	Not provided	SIMS measurement	−4.6	147	Only [100] measured. [010] and [001] estimated	−5.90
Padrón-Navarta et al. (2014)	Synthetic OH-bearing forsterite crystals	H extraction	100	800–1000	1 bar	300– 600 Bell	Polarized: A: 3613, 3572,3525 B: 3572, 3525 C: 3572, 3525	−1.1 ± 0.6	296 ± 14	[Ti] + [Si]-doped forsterite	−10.08
								3.3 ± 0.4	461 ± 11	[Si] in undoped MgO-buffered forsterite	−14.19
							Unpolarized: 3613, 3572, 3525	−4.2 ± 2.0	209 ± 45	[Mg] Previously unfitted	−8.69

Activation energy value incorrectly reported as 34 kJ/mol in Demouchy (2010a). Erratum reported in Demouchy (2012)

SCO San Carlos olivine

[a] Recalculated by Ingrin and Blanchard (2006)

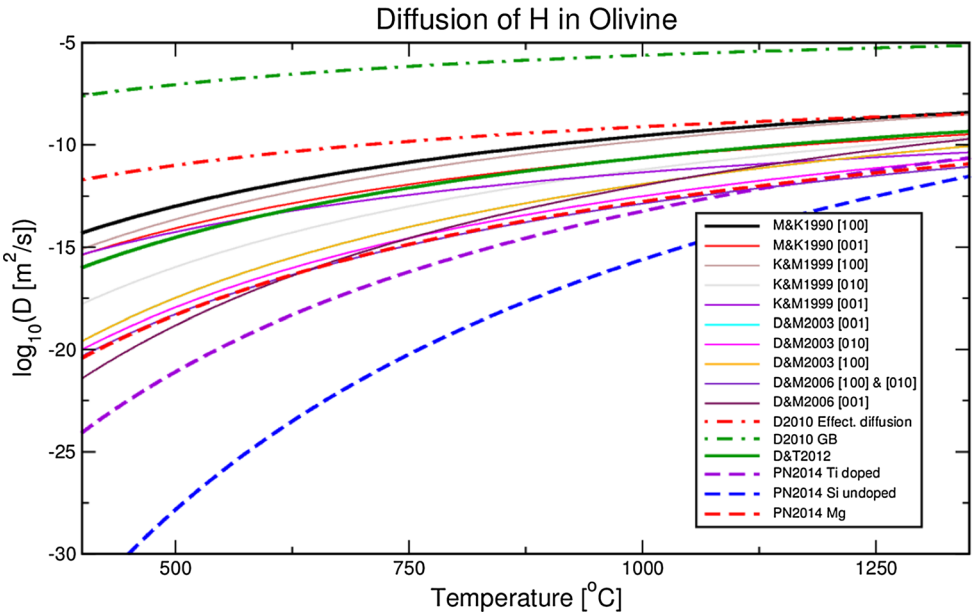

Fig. 4 Diffusion of hydrogen in olivine from published Arrhenius models. M&K1990—Mackwell and Kohlstedt (1990); K&M1999—Kohlstedt and Mackwell (1999); D&M2003—Demouchy and Mackwell (2003); D&M2006—Demouchy and Mackwell (2006); D2010—Demouchy (2010a) (with correction in Demouchy (2012)); D&T2012—Du Frane and Tyburczy (2012), recalculated by Jones (2014a); PN2014—Padrón-Navarta et al. (2014) (includes previously unpublished result for proton-Mg vacancy). See text and Table 3 for further explanation

Information of Jones (2014a), based on the databases in Farver (2010) and Brady and Cherniak (2010) (the latter is available online at *http://diffusion.smith.edu*). For each experiment, the Arrhenius parameters are given from a regression linear fit of the experimental data reporting the slope and the intercept of the data when plotted as $\log_{10}(D)$ versus $1/T$. As shown by Jones (2014a), the logarithm of the pre-exponent term (the intercept) and the activation energy (the slope) are linearly related, consistent with the Meyer–Neldel Rule (in physics) or Compensation Law (in chemistry). Adherence to that rule was recently shown to be also upheld by Si diffusion in minerals (Zhang and Shan 2015).

Diffusion rates of hydrogen in olivine calculated from published Arrhenius models are plotted in Fig. 4 for lithospheric temperatures from 400 °C (Moho for cold cratons) to 1350 °C (base of the lithosphere) for all of the Arrhenius models in Table 3. Note the extreme range of diffusion rates at mid-lithospheric temperatures (750 °C) of 15 orders of magnitude, from the slowest (*dashed blue line*, undoped Si, Padrón-Navarta et al. (2014)) to the fastest (*dash-dotted green line*, grain boundary diffusion, Demouchy (2010a)). Considering volume (grain) diffusion alone, the range is ten orders of magnitude. As I will show below, these diffusion rates translate into similar orders of magnitude difference in proton conduction through the linear Nernst–Einstein relationship between diffusion and conduction (Table 3, last column). At the higher temperatures found in the lowermost lithosphere, this range reduces to less than four orders of magnitude.

There are far fewer experiments on diffusion in pyroxenes, and all of them relate to volume diffusion. Taking the modeled Arrhenius values from the databases listed above yields the equivalent plot for diffusion rate against temperature shown in Fig. 5. Note that the range of diffusion rates is not as broad for pyroxenes as for olivines and at 750 °C is "only" some five orders of magnitude.

Volume diffusion

Lattice (or volume) diffusion is given by a standard Arrhenius equation, viz.

$$D_H^L = D_0^L \exp\left(\frac{-\Delta H^L}{RT}\right) \tag{3}$$

where D_0^L is the pre-exponent term (m^2/s), ΔH^L is the activation energy (J/mol), R is the gas constant (J/mol K), and T is the temperature (K). (Note that most of the solid-state physics community, as well as the majority of the laboratory conductivity and viscosity communities in the geosciences, report activation energy in eV, so use Boltzmann's constant on the denominator of the exponent. The diffusion community in the geosciences traditionally reports activation energy in kJ/mol so requires the gas constant on the denominator.)

The majority of the laboratory diffusion experiments were performed on single crystals, preferentially on San Carlos olivine (SCO). Thus, the diffusion measured is volume diffusion and due to either lattice diffusion or interstitial diffusion.

The most recently reported experiments by Padrón-Navarta et al. (2014) on synthetic forsterite (Fo100) crystals determined diffusion rates as a function of water residence site, [Si], [Mg], [Ti], and [triv], demonstrating that hydrogen diffusion is far more complex than previously

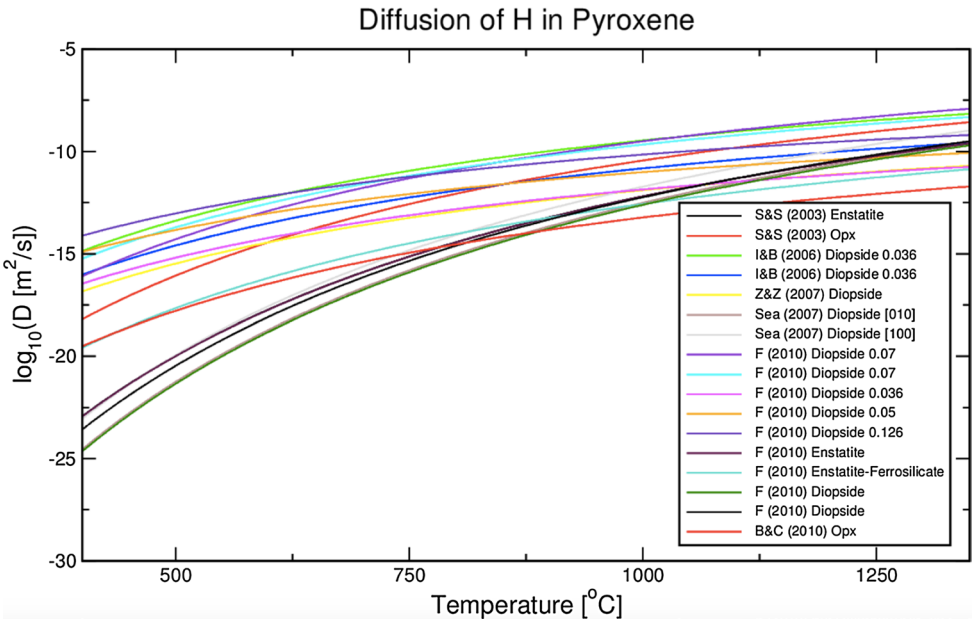

Fig. 5 Diffusion of hydrogen in pyroxene from published Arrhenius models (on same scale as Fig. 4). S&S (2003): Stalder and Skogby (2003); I&B (2006): Ingrin and Blanchard (2006) review; Z&Z (2007): Zhao and Zheng (2007) review; Sea (2009): Sundvall et al. (2009); F (2010): Farver (2010) review; B&C (2010): Brady and Cherniak (2010) online database

thought. The authors showed that the slowest diffusion was associated with Si-vacancies in undoped samples (labeled PN2014 Si undoped, *dashed blue lowest line*, Fig. 4). The next slowest was related to the interaction of Ti-hydrous defects with a fraction of the hydrated Si-vacancies (PN2014 Ti doped, *dashed purple second-lowest line*, Fig. 4). The fastest diffusion was associated with trivalent cations and Mg-vacancies (PN2014 Mg, *dashed red line*, Fig. 4). The latter falls exactly on the Demouchy and Mackwell (2006) [100] + [010] line for natural olivine (Fo90 SCO) (labeled D&M2006 [100] and [010], *solid purple line*), and parallel to, and within one-third of a log unit of (i.e., well within experimental error), the Demouchy and Mackwell (2003) [010] line for forsterite (labeled D&M2003 [010], *solid thin red line*).

The faster diffusion of trivalent and Mg H defects was also recently observed in natural olivines (Hilchie et al. 2014; Peslier et al. 2015), with the Mg H defects confirmed as yielding the fastest rates by a factor of more than 1.7, up to 6.8, over the next fastest rate, Ti-H defects, which themselves were over 1.5 orders of magnitude faster than the rates associated with Si defects (see Fig. 6, Peslier et al. 2015).

Grain boundary diffusion

It is only within the last few years that attention has focused on grain boundaries in the Earth's mantle minerals (see "Introduction" in Demouchy 2010a). In the context of this paper, grain boundary diffusion is diffusion along mineral–mineral interfaces, specifically olivine mineral interfaces. Grain boundary diffusion is also given by an Arrhenius equation,

$$D_H^{GB} = D_0^{GB} \exp\left(\frac{-\Delta H^{GB}}{RT}\right) \quad (4)$$

with the symbols taking equivalent forms as Eq. (3).

Grain boundary diffusion has been known to be far faster than volume diffusion for a century (see references in Hoffman and Turnbull 1951). In olivine, four orders of magnitude faster oxygen diffusion along grain boundaries were observed over two decades ago (Yurimoto et al. 1992). Demouchy (2010a) was the first, and to date only (as far as I am aware), experimental work on hydrogen grain boundary diffusion in olivine.

ten Grotenhuis et al. (2004) studied the electrical conductivity of dry synthetic polycrystalline forsterite at temperatures of 1180–1470 °C at low pressure (0.1 MPa), i.e., ionic conduction by Mg-vacancies. They found bulk conductivity to be inversely related to grain size, interpreted as a consequence of grain boundary diffusion of charge carriers dominating conduction. The activation energies derived resembled previously-reported data for grain boundary diffusion of Mg in forsterite by Farver et al. (1994) and also those found by Hirth and Kohlstedt (1995) in their diffusion creep experiments. The results of ten Grotenhuis et al. (2004) are discussed in further detail below.

There are no laboratory data at all on any partitioning coefficient between water in the grain and in the grain boundary films. The phrase "partition coefficient" is not used here in the normal sense of strict partitioning between, e.g., water content in olivine and water content in pyroxenes, but is used to infer how many protons are traveling on the grain boundaries compared to protons diffusing through the grains. A reasonable assumption is that the water in the

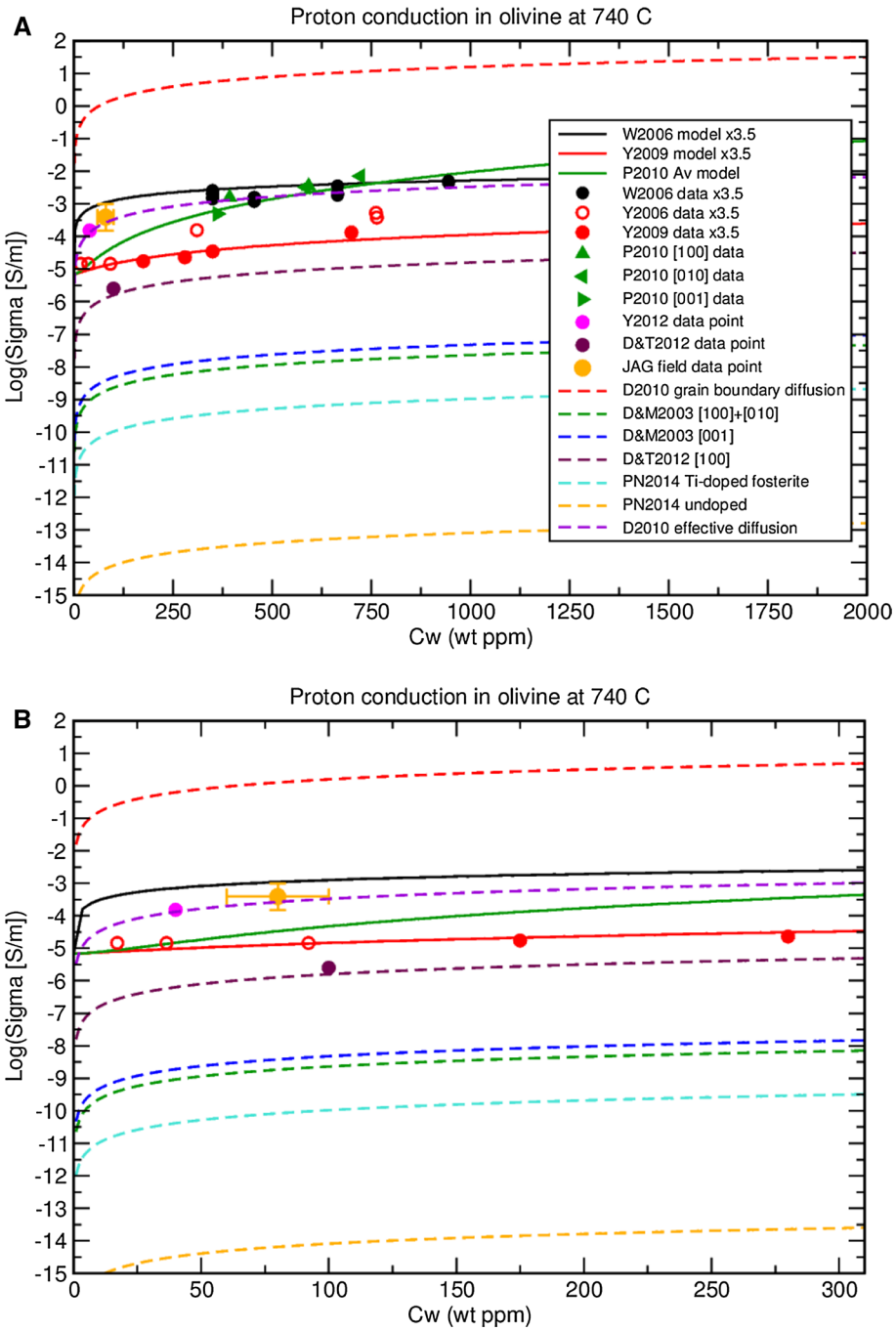

Fig. 6 Conductivity from diffusion constants listed in Table 3 compared with observations listed in Table 2 at a temperature of 740 °C for an assumed water content of 80 wt ppm. **a** 0–2000 wt ppm, **b** 0–300 wt ppm. W2006: model (*solid black line*) and data (*solid black circles*) from Wang et al. (2006) corrected to Bell calibration (×3.5). Y2006: data (*open red circles*) from Yoshino et al. (2006). Y2009: model (*solid red line*) and data (*solid red circles*) from Yoshino et al. (2009a, b) corrected to Bell calibration (x3.5). Y2012: data point (*light brown solid circle*) from Yang (2012). D&T2012: data point (*brown solid circle*) and model (*dashed brown line*) from Du Frane and Tyburczy (2012), recalculated by Jones (2014a). JAG: field data point (*yellow filled circle* with *error bars*) at 100 km below Jagersfontein kimberlite field from Jones et al. (2012). D2010: grain boundary diffusion (*dashed red line*) and effective diffusion (*dashed purple line*) rates of Demouchy (2010a) (with correction in Demouchy (2012)) converted to conductivity using the Nernst–Einstein equation. D&M2003: diffusion rates of Demouchy and Mackwell (2006) (*dashed green* and *dashed blue lines*) converted to conductivity using the Nernst–Einstein equation. PN2012: diffusion rates of Padrón-Navarta et al. (2014) for undoped (*dashed yellow line*) and Ti-doped (*dashed cyan line*) diffusion converted to conductivity using the Nernst–Einstein equation

grain boundary films is no greater than that within the grain itself, i.e., a 1:1 partitioning. I will explore below water partitioning coefficients of 1:1, 3:1 and 10:1, i.e., water in the grain boundary film of 80 wt ppm, 27 wt ppm and 8 wt ppm for 80 wt ppm in the grain, to yield a likely representative range of bulk conductivities derived from effective diffusion.

There can of course be many species on the grain boundaries. However, as discussed by Chakraborty (2010), diffusion of hydrogen is many orders of magnitude faster than any other species so we can neglect the contribution to electrical conductivity of those other possible species.

Effective diffusion

In its most general form, "effective diffusion" relates to the sum of all diffusion processes and is more typically understood to define the resulting diffusion in the lattice of two species with different diffusivities (e.g., H and polarons, or hydrogen and vacancies). In the context of this paper,

I consider effective diffusion to be bulk diffusion, i.e., the combination of lattice diffusion and grain boundary diffusion in multi-grain material (in our case not a polymineral as I am only considering in detail diffusion in olivine at this point; later I will include pyroxenes).

Demouchy (2010a, b), following Balluffi et al. (2005, p. 214), defines *effective diffusivity* as

$$D_H^{eff} = D_H^L + (3\delta/d)D_H^{GB} \tag{5}$$

where D_H^{eff} is the effective diffusivity, D_H^L is the lattice (or volume) diffusivity, D_H^{GB} is the grain boundary diffusivity, δ is the grain boundary width, usually taken to be of order 0.75 nm (two monoatomic layers) in olivine (Hiraga and Kohlstedt 2007, 2009), and d is the grain diameter.

Implicit in Eq. (5) is hydrogen partitioning between the grain and the grain boundary of 1:1. I modify Eq. (5) by adding a partition coefficient of x between grain and grain boundary water content, viz.

$$D_H^{eff} = D_H^L + x(3\delta/d)D_H^{GB}. \tag{6}$$

As stated above, this "partition coefficient" should not be thought of in the same manner as a partition coefficient of water content between various mineral species. Balluffi et al. (2005) clarifies that any proton can spend part of its transit time within the grain and the other part of the time on the grain boundary.

For what is considered to be the olivine grain size in the lithospheric mantle of the order of 10–100 μm (very fine grained in highly mylonitized and sheared zones and veins) to 1 mm (coarse grained) to 10 mm [very coarse grained, often found in xenolith material from cratons, e.g., Ave Lallemant et al. (1980), Hirth and Kohlstedt (2003)], then as D_H^{GB} is orders to many orders of magnitude greater than D_H^L, it dominates. Even for a partition coefficient x of 0.1 (i.e., 10:1 grain water content cf. grain boundary water content), D_H^{eff} is dominated by grain boundary diffusion until d is of the order of $3\,\delta D_H^{GB}/D_H^L$.

For modeling their conductivity measurements, ten Grotenhuis et al. (2004) adopt the cubic grains model of Waff (1974) derived for a sample with melt on the grain boundaries. As shown by ten Grotenhuis et al. (2004), when grain boundary conductivity (σ_{gb}) greatly exceeds grain interior conductivity (σ_{gi}) then the bulk conductivity (σ_b) can be simplified to

$$\sigma_b \approx \sigma_{gi} + \sigma_{gb}\left[1 - \left(1 - \frac{3\delta}{d}\right)^{2/3}\right], \tag{7}$$

which, for $\delta \ll d$, reduces further to

$$\sigma_b \approx \sigma_{gi} + (2\delta/d)\sigma_{gb}. \tag{8}$$

Note that here the partitioning of ionic vacancies is assumed to be 1:1. In this paper, I adopt the equation espoused by Demouchy (2010a, b), namely Eq. (5), for deriving our conductivities from effective diffusivities. The difference between the two formulae is a factor of 1.5, which is less than 0.2 log units so is well within experimental error.

At the temperatures of the mid-lithosphere, around 750–850 °C, even the fastest volume diffusion measured experimentally is some six orders of magnitude slower than grain boundary diffusion, and the slowest, which is the most common, is some 13 orders of magnitude slower (Fig. 4). Thus, volume diffusion conductivity will not begin to dominate over grain boundary conductivity until the grain size is some six orders of magnitude or more larger than the grain boundary width. Taking the latter as 1 nm this means that grain boundary conduction dominates until the grains become of order 0.1–1.0 mm.

Diffusion to conduction: the Nernst–Einstein equation

The notion of using diffusion to determine conductivity, and more particularly vice versa, has been utilized for half a century, typically using the simplest form of the Nernst–Einstein equation for non-interacting charge carriers in a unary system (Murch 1983) that relates diffusion to conduction [when the system is in thermal equilibrium (Hilt and Siebbeles 1998)] by:

$$\sigma_H = fD_H C_H q^2/kT \tag{9}$$

where σ_H is the conductivity (in S/m), f is a unitless correction correlation factor (related to the Haven ratio), usually taken as 0.5–1.0, D_H is the diffusivity of the charge carrier (in m^2/s), C_H is the concentration of the charge carrier (1/m^3), q is the charge (Coulomb), k is Boltzmann's constant (Joule/Kelvin), and T is temperature (Kelvin).

Values for proton diffusion are given in Appendix A. A full review of application of the Nernst–Einstein equation is given in Sect. 4 of the Supplementary Material.

I employ the Nernst–Einstein equation in its direct form given by Eq. (9), and for my calculations, I assume a correction correlation factor (Haven ratio) of 1.0 for full compliance. I accept that I may be in error by a factor of up to 2, but this is less than 0.3 log units and is well within experimental error, especially given the 15 orders of magnitude range of the diffusion experiments. I accept the arguments of Karato (2013) and others that volume diffusion can be by multiple species, and one must consider that hydrogen in olivine [$(Mg,Fe)_2SiO_4$] may be dissolved in the multiple forms, as discussed in the Supplementary Material (Sect. 4). However, as I show above in the discussion

of grain boundary diffusion, for grains smaller than around 1 mm at lithospheric wetting conditions (<200 wt ppm) we can ignore volume diffusion as being of second order, and we need only to consider grain boundary diffusion as it dominates.

Comparison of proton conduction experiments and hydrogen diffusion experiment predictions

Using the Nernst–Einstein relation and the Arrhenius models for hydrogen diffusion listed in Table 3, I predict the corresponding proton conduction that would be observed for lithospheric temperatures and plot them in Fig. 6 (dashed lines) for water contents of 0–2000 wt ppm (Fig. 6a) and 0–300 wt ppm (Fig. 6b) and list them in Table 3 (last column) for a temperature of 740 °C and a water content of 80 wt ppm for comparison with the JAG conductivity data at 100 km of $\log_{10}(\sigma) = -3.4 \pm 0.2$. These predictions are compared with the laboratory observations and models of proton conduction (points and solid lines), where the data and models of Wang et al. (2006) and Yoshino et al. (2006, 2009a, b) have had their water contents multiplied by 3.5 to take them from unpolarized Paterson calibration to Bell calibration.

Note that the corrected Wang et al. (2006) data (*solid black circles* in Fig. 5a) fall almost exactly on the effective diffusion line (*purple dashed line* in Fig. 5a) of Demouchy (2010a). Also, the water content corrected Wang et al. (2006) data are in better than order-of-magnitude agreement with the Poe et al. (2010) data. Only the Yoshino et al. (2006, 2009a, b) results are in serious disagreement.

Calculations of effective proton conduction

Proton conduction in single crystals of olivine will be through volume diffusion only. Thus, studies on single crystals, either diffusion studies or conductivity studies, will only measure volume diffusion. However, the real Earth is polycrystalline at a scale on the order of 0.01 to 10 mm, so one must be cognizant of grain boundary effects as well as volume effects. Clearly, proton conduction in polycrystalline rocks will be by effective diffusion, combining grain boundary diffusion and lattice diffusion by

$$\begin{aligned}\sigma_H^{eff} &= fD_H^{eff} C_H q^2/kT \\ &= f\left(D_H^L + x(3\delta/d)D_H^{GB}\right)C_H q^2/kT \\ &= f\left(D_0^L \exp\left(\frac{-\Delta H^L}{RT}\right)\right. \\ &\quad \left. + x(3\delta/d)D_0^{GB}\exp\left(\frac{-\Delta H^{GB}}{RT}\right)\right)C_H q^2/kT. \end{aligned} \quad (10)$$

If I take D_0^L and ΔH^L from Du Frane and Tyburczy (2012) (note that it does not matter which lattice diffusion model I adopt for small grains (<0.1 mm), as grain boundary diffusion dominates by orders of magnitude, even for values of x of order 0.1), and D_0^{GB} and ΔH^{GB} from Demouchy (2010a) ($\log_{10}(D_0^{GB}) = -3.4$, $\Delta H^{GB} = 54$ kJ/mol), then σ_H^{eff} predicted at 740 °C for a water content of 80 ± 20 ppm for $x = 1.0$ (unity partition coefficient), $\delta = 1$ nm and $d = 0.001$, 0.01, 0.1, 1.0, and 10 mm yields log(conductivities) of −2.4 to −5.8, as listed in Table 4 and shown in Fig. 7.

Total conductivity

Within dry silicate rocks in the lithospheric mantle, there are two conduction processes operating, namely small polaron conduction and ion vacancy conduction. The former of these dominates at low temperatures (shallow depths) and the latter at high temperatures (deeper depths), with the latter becoming more important at temperatures of order 1250 °C (Fig. 2), i.e., toward the base of the lithosphere. However, as shown in Fig. 2 both effects must be considered at temperatures in excess of around 1000 °C. When there is water present, then proton conduction must also be considered.

The total conductivity of a polycrystalline rock comprises volume effects and grain boundary effects. Grain boundary effects caused by ionic conduction were studied and reported by ten Grotenhuis et al. (2004), and grain boundary diffusion of hydrogen by *Demouchy* (2010a, 2012). Taking these all together yields a new equation for the conductivity of olivine that takes all conduction mechanisms and both grain and grain boundary effects into account:

$$\sigma = \sigma_{sp,l} + \left(\sigma_{p,l} + x(3\delta/d)\sigma_{p,gb}\right) + \left(\sigma_{i,l} + (3\delta/d)\sigma_{i,gb}\right) \quad (11)$$

where subscripts *sp*, *p*, and *i* refer to small polaron, proton, and ionic conduction, respectively, subscripts *gb* and *l* refer to grain boundary and lattice conduction, respectively, and x denotes the water partition coefficient in olivine between grains and grain boundaries. These terms are:

$$\begin{aligned}\sigma_{sp} &= \sigma_{0h}\exp\left(\frac{-\Delta H_h}{kT}\right) \\ &= \left(\frac{10^{6.54}}{T}\right)X_{Fe}^{1.81}\exp\left(\frac{-1.35}{\left(8.617\times10^{-5}\right)\times T}\right)(S/m), \end{aligned} \quad (12)$$

where X_{Fe} is the iron number (Fe/Fe+Mg) and T is temperature in Kelvin.

Table 4 Electrical conductivity at 100 km for temperature of 740 °C beneath Jagersfontein compared to calculations from proton conduction models and from effective diffusion models

Source	$\log_{10}(D_0^L)$ (m^2/s) or for conductivity σ_0 (S/m) and r	E^L (kJ/mol) or for conductivity E (eV) and α(ev/(wt ppm)$^{1/3}$)	$\log_{10}(D_H^L)$ (m^2/s)	$\log_{10}(D_H^{GB})$ (m^2/s)	d (mm)	$\log_{10}(D_H^{eff})$ (m^2/s)	$\log_{10}(\sigma)$ (S/m)	Comments
Jagersfontein observation Jones et al. (2012)	–	–	–	–	–	–	−3.4 ± 0.2	T estimated as 740 ± 50 °C, P estimated as 3.2 GPa
Wang et al. (2006) proton conduction model	3.0 ± 0.2 0.62 ± 0.15	0.87 ± 0.05 *0 (fixed)*	–	–	0.5–2.0	–	−2.96	Model from paper x3.5 to account for unpolarized FTIR spectra with Paterson calibration, i.e., calculated for Cw = 80/3.5 = 23 ppm
Yoshino et al. (2009) proton conduction model	1.9 ± 0.44 *1 (fixed)*	0.92 ± 0.04 0.16 ± 0.02	–	–	Compacted fine powder	–	−5.21	Model from paper x3.5 to account for unpolarized FTIR spectra with Paterson calibration, i.e., calculated for Cw = 80/3.5 = 23 ppm
Poe et al. (2010) average proton condu ction model	2.35 ± 0.11 *1 (fixed)*	1.19 ± 0.035 1.10 ± 0.055	–	–	Single crystal	–	−4.57	Bell calibration Single crystal, so only lattice diffusion. Should be same as calculated from lattice diffusion expts.
Yang (2012) [100] proton conduction model	0.93 ± 0.26 No Cw	0.95 ± 0.04 *0 (fixed)*	–	–	–	–	−3.50 ± 0.2	−3.80 ± 0.28 Single point for Cw = 40 ppm Bell calibration Adjusted to 80 ppm by multiplying by 2
Demouchy and Mackwell (2006) [100] and [010] diffusion model	−4.5	204	−15.0	−6.18	0.001	−8.7	−2.4	
					0.01	−9.7	−3.4	Exactly the JAG value
					0.1	−10.7	−4.4	
					1	−11.7	−5.4	
					10	−12.7	−6.4	
Du Frane and Tyburczy (2012) [100] diffusion model	−4.6	147	−12.2	−6.18	0.001	−8.7	−2.4	
					0.01	−9.7	−3.4	Exactly the JAG value
					0.1	−10.7	−4.4	
					1	−11.6	−5.3	
					10	−12.1	−5.8	

Table 4 continued

Source	$\log_{10}(D_0^L)$ (m^2/s) or for conductivity σ_0 (S/m) and r	E^L (kJ/mol) or for conductivity E (eV) and α(ev/(wt ppm)$^{1/3}$)	$\log_{10}(D_H^L)$ (m^2/s)	$\log_{10}(D_H^{GB})$ (m^2/s)	d (mm)	$\log_{10}(D_H^{diff})$ (m^2/s)	$\log_{10}(\sigma)$ (S/m)	Comments
Gardes et al. (2015) "unified hydrous olivine conduction law"	2.75 ± 0.45 *1 (fixed)*	0.92 ± 0.07 0.22 ± 0.005	–	–	–	–	−3.72	Model derived through fitting laboratory data with very large errors on the water contents to accommodate bias error

$$
\begin{aligned}
\sigma_p &= \sigma_{p,l} + x(3\delta/d)\sigma_{p,gb} \\
&= f\left(D_0^L \exp\left(\frac{-\Delta H^L}{RT}\right) + x(3\delta/d)D_0^{GB}\exp\left(\frac{-\Delta H^{GB}}{RT}\right)\right)C_H q^2/kT \\
&= f\left(\begin{array}{c} 10^{-4.6}\exp\left(\frac{-147\times10^3}{8.31\times T}\right)+ \\ x(3\delta/d)10^{-3.4}\exp\left(\frac{-54\times10^3}{8.31\times T}\right) \end{array}\right) \\
&\quad\times\left(\frac{6.2214\times10^{23}\rho}{153.3}\left(\frac{C_w}{10^6}\right)\right) \\
&\quad\times\left(1.602\times10^{-19}\right)^2/\left(\left(1.3805\times10^{-23}\right)\times T\right)
\end{aligned}
\tag{13}
$$

where f is the correction correlation factor (usually in the range 0.5–1.0, here assumed to be 1.0), x is the water partition coefficient between grains and grain boundaries, δ is the grain boundary width (taken to be 1 nm (Farver et al. 1994)), d is the grain diameter, and ρ is the density of olivine (here assumed to be 3.32 10^6 g/m^3), and I have adopted the lattice diffusion Arrhenius coefficients of Du Frane and Tyburczy (2012).

$$
\begin{aligned}
\sigma_i &= \sigma_{i,l} + (3\delta/d)\sigma_{i,gb} \\
&= \sigma_{0i}^L \exp\left(\frac{-\Delta H_i^L}{kT}\right) + (3\delta/d)\sigma_{0i}^{GB}\exp\left(\frac{-\Delta H_i^{GB}}{kT}\right) \\
&= 10^{4.73}\exp\left(\frac{-2.31}{\left(8.617\times10^{-5}\right)\times T}\right) \\
&\quad + (3\delta/d)10^{6.8}\exp\left(\frac{-220\times10^3}{8.31\times T}\right),
\end{aligned}
\tag{14}
$$

where k is in eV/K in the first term, δ and d are the same values as above, the activation energy for grain boundary diffusion is reported in kJ/mol by ten Grotenhuis et al. (2004), so the denominator includes the gas constant R, and the pre-exponent term in the ionic grain boundary conductivity has been estimated from the plots in ten Grotenhuis et al. (2004) as the term was not reported.

The interior ionic conduction term adopted here, $\sigma_{i,l}$, is the one preferred by Fullea et al. (2011) and comes from the work of Yoshino et al. (2009). This conduction term is some two orders of magnitude smaller than the grain boundary term, $\sigma_{i,gb}$, so for all reasonable grain sizes interior conduction is far larger than $(3\delta/d)\sigma_{i,gb}$ grain boundary conduction (by more than an order of magnitude). This result is counter to that of ten Grotenhuis et al. (2004), who assumed five orders of magnitude difference in conductivity based on the diffusion data of Farver et al. (1994). More attention needs to be paid to ion conduction by Mg-vacancies, especially given the queries raised about the proton conduction results in Yoshino et al. (2009a, b). For this paper, as I focus on lower temperatures of 740–850 °C

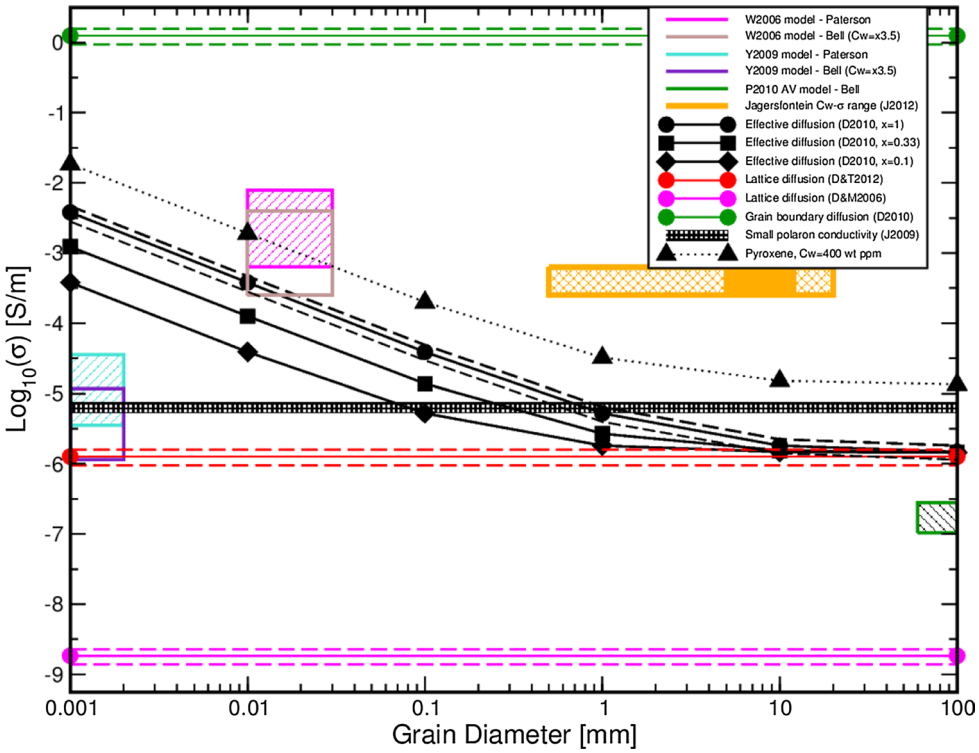

Fig. 7 Total Nernst–Einstein derived conductivity for various grain sizes from 0.001 mm (1 nm) to 100 mm and for varying partition coefficient x, plus laboratory and field observations for a temperature of 740 °C and a water content of 80 (±20) wt ppm. D2010 (*green line*): Conductivity from grain boundary diffusion (Demouchy 2010a, 2012); D&T2012 (*red line*): Conductivity from lattice diffusion using the Arrhenius parameters of Du Frane and Tyburczy (2012); D&M2006 (*purple line*): Conductivity from lattice diffusion using the Arrhenius parameters of Demouchy and Mackwell (2006); D2010 (*black lines*): Effective conductivity based on grain boundary diffusion of Demouchy (2010a; 2012) plus lattice diffusion of Du Frane and Tyburczy (2012). *Black line* with *filled circles*: effective conductivity from grain boundary diffusion plus lattice diffusion (see text for details) for a partition coefficient of 1:1; *dashed lines* on either side denote ±20 wt ppm. *Black line* with *filled squares* and *filled diamonds*: effective conductivity from grain boundary diffusion plus lattice diffusion (see text for details) for partition coefficients x of 3:1 and 10:1, respectively. (Note that (1) effective diffusion approximation invalid for $d < 0.01$ mm when grain diameter becomes of order grain film width, (2) at large grain sizes then polaron conduction becomes important and for large partition coefficients dominates.) *Black line* with *filled triangles*: effective conduction from grain boundary diffusion plus lattice diffusion in pyroxenes (partition coefficient of 1:1) W2006 (*purple shaded box*): conductivity extrapolated from laboratory experiments of Wang et al. (2006) adopting their formula using samples formed from grains of 10–30 μm, with Paterson water calibration; (*brown box*): Conductivity extrapolated from laboratory experiments of Wang et al. (2006) adopting their formula using samples with grains of 10–30 μm, with Bell water calibration. Y2009 (*turquoise shaded box*): Conductivity extrapolated from laboratory experiments of Yoshino et al. (2009a, b) adopting their formula using samples formed from ground particles of <1 μm, with Paterson water calibration; (*purple box*): conductivity extrapolated from laboratory experiments of Yoshino et al. (2009a, b) adopting their formula using samples formed from ground particles of 1 nm, with Bell water calibration. P2010 (*green shaded box*): averaged conductivity extrapolated from laboratory experiments of Poe et al. (2010) adopting their formula using single grain samples, with Bell calibration. J2012 (*orange hashed box*): conductivity range at 100 km below the Jagersfontein kimberlite field ($\log_{10}(\sigma) = -3.4 \pm 0.2$ S/m) (Jones et al. 2012) for averaged grain sizes in the lithosphere generally (0.5–20 mm) and in the Kaapvaal Craton specifically (7–12 mm, *solid orange box*, Ave Lallemant et al. 1980). J2009 (*black hashed line*): conductivity of small polaron conduction from Jones et al. (2009) formula

where ion conduction is secondary, this discrepancy is immaterial, but the terms are included in Eq. (14) for completeness.

Comparison with average grain size in the lithospheric mantle

Knowing the grain size in the upper mantle is crucial for estimating its rheological properties (Karato and Wu 1993). For small grains, where "small" is relative and is a function of stress, strain, temperature, and pressure, deformation occurs through diffusion creep and strain rate increases linearly with stress. In contrast, for large grains, again where size is relative, deformation occurs through dislocation creep, and strain rate is nonlinear with respect to stress (Karato and Wu 1993). Figure 4 of Karato and Wu (1993) shows these effects for a nominal grain size of 1 mm. Our only observations on grain size come from xenolith material exhumed from the upper mantle, and estimates of the grain size are thought to possibly show sample bias toward

smaller grain sizes on average (Ave Lallemant et al. 1980; Behr and Hirth 2014).

Coupling together knowledge of effective diffusion as the sum of lattice and grain boundary diffusion and determining the effective conductivity, i.e., parallel conductivity, from effective diffusion using the Nernst–Einstein relationship, we are able obtain an estimate the average grain size of interconnected most conducting paths within the lithospheric mantle at 100 km below the Jagersfontein kimberlite field from our MT observations and compare that with the grain sizes found in xenoliths. Note that, as discussed by Karato (2013) (see above), electrical conductivity is governed by the fastest conduction process, so conductivity-based estimates of grain size will be biased toward the average of the smallest partially interconnected grains and should not be used to estimate average grain size sensu stricto.

Figure 7 shows the proton conductivity derived from lattice diffusion along the [100] direction estimated by Du Frane and Tyburczy (2012) (*red solid* and *dashed lines* labeled D&T2012, where the *solid line* is for 80 wt ppm and the *bounding dashed lines* are for 60 and 100 wt ppm), conductivity derived from lattice diffusion along the [100] + [010] directions estimated by Demouchy and Mackwell (2006) (*purple solid* and *dashed lines* labeled D&M2006), conductivity from grain boundary diffusion estimated by Demouchy (2010b) (*green solid* and *dashed lines* labeled D2010), small polaron conductivity from Jones et al. (2009) (*black hatched line* labeled J2009), and the effective diffusion for varying grain size (*black solid* and *dashed lines* labeled D2010), all for a water content in olivine of 80 ± 20 ppm and a water partitioning of 1:1. The conductivities for other water partition coefficients are shown by the two *black lines* with *square symbols* (3:1 partitioning, i.e., 27 wt ppm water in the grain boundaries) and *diamond symbols* (10:1 partitioning, i.e., 8 wt ppm water in the grain boundaries). Also shown is the range of the conductivity below Jagersfontein at 100 km, namely $\log_{10}(\sigma) = -3.4 \pm 0.2$, for the general range of expected grain sizes within cratonic lithosphere of 0.5–20 mm (*orange hatched region*) and the 5–12 mm range grain sizes of olivines recovered from xenoliths on the Kaapvaal Craton (Ave Lallemant et al. 1980, their Fig. 7) (*orange solid region*).

Note that the gradient of the diffusion rate with water content is relatively small except at very low values, of order <15 wt ppm (see Fig. 5b). Hence, conductivity will be reduced with lower water contents, but a reduction in water content by a factor of three, from 80 to 27 wt ppm, only reduces the effective conductivity by 0.5 log units (i.e., a linear factor of 3).

Also shown in Fig. 7 are the ranges of conductivities determined from the proton conduction models of Wang et al. (2006) (*hatched magenta box* and *brown box* labeled W2006), Yoshino et al. (2009a, b) (*hatched turquoise box* and *purple box* labeled Y2009) and Poe et al. (2010) (*hatched green box* labeled P2010 AV); the ranges were derived through bootstrapping a million realizations using the laboratory-determined Arrhenius parameters and their errors (as listed in Table 1) reported by the respective authors. The former two are plotted with two ranges, one for the reported models (*hatched boxes*) and the second for the models corrected to Bell calibration (x3.5) (*unfilled boxes*). In the case of Wang et al. (2006), the samples were polycrystalline olivine grains with grain sizes of 10–30 μm. For Yoshino et al. (2009a, b), the SCO grains were powdered to extremely fine power and then reconstituted. For Poe et al. (2010), single crystals of olivine were used.

Note that the Wang et al. (2006) field falls exactly on the effective diffusion prediction line for 80 wt ppm grain and grain boundary diffusion expected for such grain sizes. The Poe et al. (2010) conductivity field falls between the conductivity predictions of volume diffusion of Du Frane and Tyburczy (2012) and of Demouchy and Mackwell (2006), as expected for single crystals without grain boundary diffusion. Puzzling is the Yoshino et al. (2009a, b) conductivity field—far higher conductivity is expected given that the samples comprised pressed μm powder.

The effective diffusion line for 80 wt ppm and the Jagersfontein conductivity line do not intersect for grain sizes of 0.5–20 mm. Intersection occurs for 80 wt ppm at grain sizes of 0.01 mm. This implies that if proton conduction in olivine with 80 wt ppm water is the cause of the enhanced conductivity beneath Jagersfontein, then the most conducting pathways are along very fine-grained olivines. Alternatively, the pathways could be along well-interconnected fine-grained (0.05 mm) pyroxenes (*dotted black line* with *filled triangles*): Orthopyroxenes have measured water contents up to 200 wt ppm and clinopyroxenes, although low in abundance, with double that, up to 400 wt ppm (Grant et al. 2007). Veins of high water content finer-grained pyroxenes and even phlogopite have been observed in coarse-grained Tanzanian xenoliths (Baptiste et al. 2015); if extensive, such veins could form well-connected conductive pathways and hence enhance conductivity.

Figure 2 shows a comparison of various conduction processes and field data from 100 km below the Jagersfontein (JAG, South Africa) and Gibeon (GIB, Namibia) kimberlite fields. The Jagersfontein data ($\log_{10}(\sigma) = -3.4$) are fully explained by 80 wt ppm water in olivine and grain boundary diffusion, with grains of 0.01 mm on average, at a temperature of 740 °C (thick solid red line, Fig. 2), or of 400 wt ppm water in pyroxenes (thick dashed black line, Fig. 2). However, the Gibeon data ($\log_{10}(\sigma) = -2.8$) are not fit by 80 wt ppm water at 850 °C for grains of 0.01 mm or by 400 wt ppm water for grains of 0.05 mm. This means that one of four possibilities exists:

1. For the same grain size (0.01 mm) and olivine water content (80 wt ppm), the ambient temperature is far

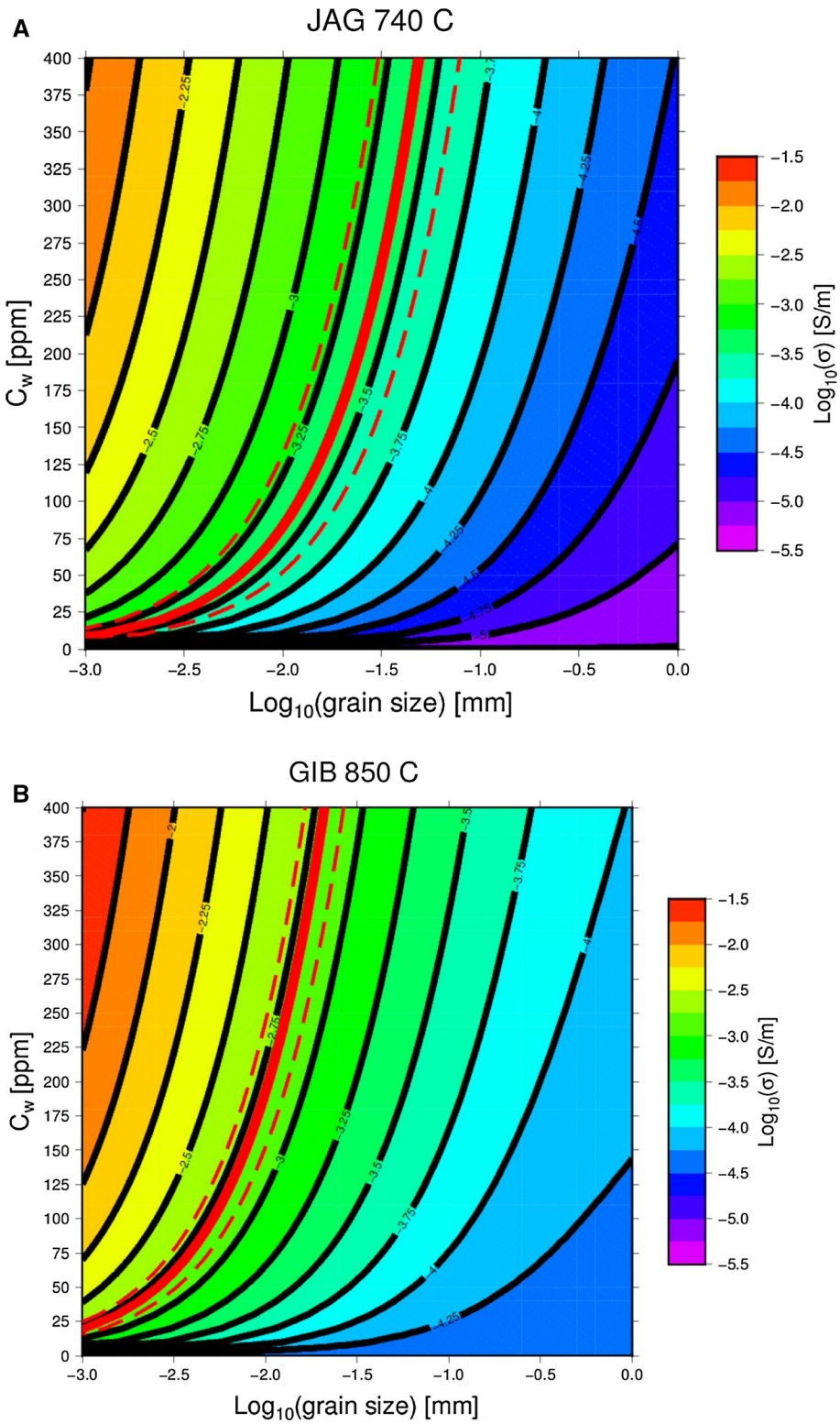

Fig. 8 **a** Total conductivity at 740 °C for Mg# of 93.0 (conditions at 100 km beneath the Jagersfontein kimberlite field, Kaapvaal Craton, South Africa) as a function of grain size and water content. The observed conductivity is $\log_{10}(\sigma) = -3.4 \pm 0.2$ S/m (*solid red line*, with the error range shown by the two *dashed red lines*). **b** Total conductivity at 850 °C for Mg# of 91.75 (conditions at 100 km beneath the Gibeon kimberlite field, Rehoboth terrane, Namibia) as a function of grain size and water content. The observed conductivity is $\log_{10}(\sigma) = -2.8 \pm 0.1$ S/m (*solid red line*, with the range shown by the two *dashed red lines*)

higher than that estimated and is of order 1040 °C. This is highly unlikely as the temperature at eruption of the Group I kimberlites some 75–65 Myr ago is estimated to be of the order of 965–1000 °C (Schmädicke et al. 2011), and there is no record of any further heating since.

2. For the same grain size (0.01 mm) and inferred temperature (850 °C), the water content is higher than that observed below Jagersfontein, and a value of 200 wt ppm in olivine is required to fit the GIB data point. This is just possible given solubility arguments, and

possible given the location of the Gibeon kimberlite field on the edge of the Rehoboth terrane and close to a continent-ocean margin.

3. For the same olivine water content (80 wt ppm) and inferred temperature (850 °C), the grain size is smaller than that beneath Jagersfontein, and a grain size of 0.004 mm of the most conducting phase on average would fit.
4. Or some combination of two or all three of them; for example, a slightly warmer ambient temperature of 900 °C with somewhat wetter olivine of 120 wt ppm with slightly smaller average grain size of 0.008 mm fits the GIB data point.

The trade-off between grain size and water content is shown in Fig. 8 for (A) a temperature of 740 °C and an Mg# of 93.0, i.e., Jagersfontein (JAG) conditions at 100 km, and (B) a temperature of 850 °C and a Mg# of 91.75, i.e., Gibeon (GIB) conditions also at 100 km. The two contour plots show the total conductivity (small polaron conduction plus volume diffusion plus grain boundary diffusion plus ion conduction) as a function of grain size and water content. The acceptable ranges are bounded by (A) the two *dashed red* contour intervals at −3.6 and −3.2, given that the observed conductivity at 100 km beneath the Jagersfontein kimberlite field is $\log_{10}(\sigma) = -3.4 \pm 0.2$ S/m, and (B) the two *dashed red* contour intervals at −2.7 and −2.9, given that the observed conductivity at 100 km beneath the Gibeon kimberlite field is $\log_{10}(\sigma) = -2.8 \pm 0.1$ S/m (Jones 2014b). Note that beyond a given grain size, around 0.02 mm for JAG and 0.01 mm for GIB, within the limits of the observation conductivity is insensitive to water content in excess of around 200 wt ppm. This sensitivity is true at all temperatures and scales inversely with grain size. At low water contents, less than 20 wt ppm, then conductivity is far less sensitive to water content but highly sensitive to grain size, down to very small grain sizes of 0.002 mm below which the conductivities virtually coalesce.

Discussion and conclusions

Proton conduction through the diffusion of hydrogen, the fastest diffusing species by far, was proposed some 25 years ago to be a significant cause of enhanced conductivity in the mantle (Karato 1990). However, the most recent volume diffusion experiments on olivine show that the diffusion rates are highly dependent on the storage location within the lattice (Padrón-Navarta et al. 2014), but that for none of them is the diffusion rate high enough, by many orders of magnitude, to explain the observed enhancements in conductivity in the polycrystal experiments of Wang et al. (2006) or of the field observations. Indeed, at the temperatures found in the lithospheric mantle, polaron conduction (*thin solid black line*, underlies *thick solid red line* at low temperatures, Fig. 2) dominates over lattice proton conduction (*thin dashed purple line*, Fig. 2) by more than an order of magnitude for lower temperatures (<1100 °C), and ion conduction (*thin blue line*, Fig. 2) dominates over lattice proton conduction by more than an order of magnitude at higher temperatures (>1100 °C).

Diffusion of hydrogen occurs within the grains, by volume diffusion, and also on the grain boundaries, and the two taken together is defined as bulk or effective diffusion. Grain boundary diffusion is many orders of magnitude faster than volume diffusion (Demouchy 2010a, 2012). Comparing the diffusion rates within olivine, the dominant mantle mineral, at mid-lithosphere temperatures for grain boundary diffusion and diffusion of hydrogen from the most common lattice site, with an assumed partition coefficient of 1:1 grain boundary diffusion dominates until the average grain becomes of a size equivalent to the magnitude difference between grain and grain boundary diffusion, i.e., some six orders of magnitude greater than the grain boundary width, which is of order 0.1–1 mm (Fig. 7).

Laboratory studies on proton conduction in olivine in general demonstrate a significant difference in results between polycrystal samples and whole grain samples, with the former far more conducting than the latter, inferring the role of grain boundary diffusion effects (see Table 1 and Fig. 3). In particular and of note, Karato and co-workers have almost exclusively used polycrystals, except for their most recent publication (Dai and Karato 2014a). Measurements on the SCO single crystal with a water content of 460 wt ppm Paterson calibration, which is approximately 1600 wt ppm Bell calibration, yield $\log_{10}(\sigma)$ values of −3.6 ([001]) to −2.6 [100]) at 740 C (Table 3), with a geometric mean of −2.9 (*down solid triangle*, Fig. 3). This compares with the far higher conductivities, by over 1.5 orders of magnitude, observed in earlier experiments on olivine polycrystals by Wang et al. (2006) (*solid black circles*, Fig. 3).

The two laboratory results that are inconsistent with the thesis of this paper are (1) those of Yoshino et al. (2009a, b) on sintered powdered samples that are far too resistive, indicative of lattice diffusion only, and (2) those of Yang (2012) on single crystals that are far too conductive, indicative of grain boundary diffusion. These cannot be explained within this framework.

Knowing the effects on electrical conductivity of water in the lithospheric mantle is key if results from deep-probing magnetotelluric studies are to be confidently interpreted. The three main laboratories conducting the measurements appear at first sight not to be in agreement. However, when the differences in the samples are

considered, then the measurements the Karato group (Wang et al. 2006) and of Poe's laboratory (Poe et al. 2010) are in agreement when diffusion at grain boundaries is included. As stated above, disparate with these measurements and observations are the measurements from Yoshino's laboratory (Yoshino et al. 2009a, b). These can only be explained in terms of volume diffusion only, which is at odds with the nature of their sample preparation.

In addition, examination of the FTIR spectra from the prior conductivity experiments shows dominance by Si-vacancies, and the diffusion process associated with this water residence site is many, many order of magnitude too slow to explain the observed conductivities. The sole exception is that of Yang (2012), with spectra that show faster diffusion processes. However, those alone are insufficient to explain the high conductivity observed.

Knowing the electrical conductivity with high precision, and having reasonable estimates of temperature and water content, one can estimate the average grain size in the lithosphere of the most conducting process to compare with xenolith observations. Considering the well-calibrated conductivities and well-estimated temperatures at 100 km beneath two kimberlite fields in southern Africa, I show that beneath the Jagersfontein field on the Kaapvaal Craton the inferred average grain size is some 0.01 mm, for 60–100 wt ppm water in the olivine, or 0.05 mm for 200–400 wt ppm water in pyroxenes. This is inconsistent with the 5–12 mm observed in xenoliths, which implies either that conduction is along well-interconnected very fine-grained material, possibly in mylonitized veins, or that another conduction mechanism dominates than proton conduction in olivine. I posit that veins of fine-grained pyroxenes may be responsible.

With regard to the proton conduction experiments, it is clear that an agreed universal protocol must be established for the laboratories to follow. Pommier (2014) discusses some aspects and makes recommendations for improvements in her excellent review.

The following specific recommendations are made with regard to using FTIR spectra. For calculations of total absorbance: for single crystal measurements use the polarized light along principal directions (Libowitzky and Rossman 1996) and for polycrystalline aggregates of small grain sizes (much lower than the aperture used for FTIR measurements, typically 50–100 microns) use the method of Sambridge et al. (2008) and Kovacs et al. (2008) if the maximum linear absorbance is lower than 0.3. For calibration of the spectra to determine water content, use the calibration of Bell et al. (2003) for Ti-point defects or Withers (2013) for Si-vacancies and for all Group I bands.

Acknowledgments The author wishes to sincerely thank Andrea Tommasi and Sylvie Demouchy for all their patient guidance over the last five years (2010–2014) during my annual month-long sabbatical visits every Spring to Université Montpellier 2, and Jose Alberto Padron-Navarta for his mentoring and information during the last visit (2014). Particularly, Sylvie's and Jose Alberto's advice and discussions were key to the development of this paper, and Jose Alberto is profusely thanked for his generous direction on the details of FTIR spectra and diffusion that appear in this paper, and in particular for his comments on the reviews of an earlier version of this paper. Dr. Wyatt Du Frane is also thanked for comments on an earlier version of this paper and for his readiness and willingness to engage with the author regarding some of the points he raised. In particular, Du Frane encouraged adoption of a partition coefficient relating water in the olivine grains to water in the grain boundaries. Dr. Anne Peslier made substantial comments on the submitted version of the manuscript, all of which helped improve it, and the editor, Catherine McCammon, gave substantial guidance. Finally, discussions with Professors Fabrice Gaillard and Shun Karato subsequent to presentation of these ideas at the 2015 EGU and IUGG meetings also provided important ideas that aided in making the concepts more robust. Funding support for the visits by AGJ came from SFI and IRCSET project support (SFI grants 07/RFP/GEOF759 and 10/IN.1/I3022, and an IRCSET grant for TopoMed), a Science Foundation Ireland Short Term Travel Fellowship award, an IRCSET Ulysses award, and funding from the Université Montpellier 2. All bodies are gratefully acknowledged. All data discussed in this paper are listed in the tables and are available from the cited references.

Appendix A

Calculation of proton conductivity from the Nernst–Einstein equation

The simple Nernst–Einstein equation is

$$\sigma_H = fD_H C_H q^2/kT. \tag{A1}$$

To compute the conductivity for proton conduction due to hydrogen diffusion, then

σ_H is the predicted proton conduction conductivity (in S/m).

f is a unitless correction correlation factor (related to the Haven ratio), usually taken as 0.5–1.0.

D_H is the diffusivity of the charge carrier (m^2/s). This is given by an Arrhenius equation of the form $D_H = D_0 \exp(-\Delta H/RT)$, where D_0 is the pre-exponent term, ΔH is the activation energy in J/mol, and R is the gas constant (8.3144621 Joule/mol Kelvin).

C_H is the concentration of the charge carrier ($1/m^3$). This is obtained from the wt ppm of water in the olivine, C_w, from $C_H = N_A \rho C_f/M$, where N_A is Avogadro's number (gas constant divided by Boltzmann's constant, R/k, 6.0221415 10^{23}/mol), ρ is the density of olivine (taken as 3.32 10^6 g/m^3 in the calculations performed herein), C_f is the fractional water content, given by $C_w/10^6$, and M

is the molecular weight of olivine (153.3 g/mol).

q is the charge (Coulomb). For a proton, this is $1.602\ 10^{-19}$ Coulomb.

k is Boltzmann's constant ($1.3805\ 10^{-23}$ Joule/Kelvin).

T is temperature (Kelvin).

References

Ahrens TJ (1989) Planetary origins—water storage in the mantle. Nature 342:122–123. doi:10.1038/342122a0

Aines RD, Rossman GR (1984) Water in minerals? A peak in the infrared. J Geophys Res 89:4059–4071. doi:10.1029/JB089iB06p04059

AveLallemant HG, Mercier JCC, Carter NL, Ross JV (1980) Rheology of the upper mantle—inferences from peridotite xenoliths. Tectonophysics 70:85–113. doi:10.1016/0040-1951(80)90022-0

Bai Q, Kohlstedt DL (1992) Substantial hydrogen solubility in olivine and implications for water storage in the mantle. Nature 357:672–674

Bali E, Bolfan-Casanova N, Koga KT (2008) Pressure and temperature dependence of H solubility in forsterite: an implication to water activity in the Earth interior. Earth Planet Sci Lett 268:354–363. doi:10.1016/j.epsl.2008.01.035

Balluffi RW, Allen SM, Carter WC (2005) Kinetics of materials. Wiley, Hoboken

Baptiste V, Tommasi A, Vauchez A, Demouchy S, Rudnick RL (2015) Deformation, hydration, and anisotropy of the lithospheric mantle in an active rift: constraints from mantle xenoliths from the North tanzanian divergence of the East African Rift. Tectonophysics 639:34–55. doi:10.1016/j.tecto.2014.11.011

Behr WM, Hirth G (2014) Rheological properties of the mantle lid beneath the Mojave region in southern California. Earth Planet Sci Lett 393:60–72. doi:10.1016/j.epsl.2014.02.039

Bell DR, Rossman GR (1992) Water in earth's mantle: the role of nominally anhydrous minerals. Science 255:1391–1397

Bell DR, Rossman GR, Maldener J, Endisch D, Rauch F (2003) Hydroxide in olivine: a quantitative determination of the absolute amount and calibration of the IR spectrum. J Geophys Res Solid Earth. doi:10.1029/2001jb000679

Beran A, Zemann J (1969) Über (OH)-Gruppen in olivin Anzeiger—Österreichische Akademie der Wissenschaften, Mathematisch-naturwissenschaftliche Klasse 106:73–74

Berry AJ, Hermann J, O'Neill HSC, Foran GJ (2005) Fingerprinting the water site in mantle olivine. Geology 33:869–872. doi:10.1130/g21759.1

Berry AJ, O'Neill HSC, Hermann J, Scott DR (2007) The infrared signature of water associated with trivalent cations in olivine. Earth Planet Sci Lett 261:134–142. doi:10.1016/j.epsl.2007.06.021

Bolfan-Casanova N (2005) Water in the Earth's mantle. Mineral Mag 69:229–257. doi:10.1180/0026461056930248

Brady JB, Cherniak DJ (2010) Diffusion in minerals: An overview of published experimental diffusion data. In: Zhang YX, Cherniak DJ (eds) Diffusion in minerals and melts, vol 72. Reviews in mineralogy and geochemistry. Mineralogical society of America, Chantilly, VA 20151-1110, United States pp 899–920. doi:10.2138/rmg.2010.72.20

Chakraborty S (2010) Diffusion coefficients in olivine, wadsleyite and ringwoodite. In: Diffusion in minerals and melts, vol 72. Reviews in mineralogy and geochemistry. pp 603–639. doi:10.2138/rmg.2010.72.13

Chu X, Korenaga J (2012) Olivine rheology, shear stress, and grain growth in the lithospheric mantle: geological constraints from the Kaapvaal craton. Earth Planet Sci Lett 333:52–62. doi:10.1016/j.epsl.2012.04.019

Dai L, Karato S-I (2009) Electrical conductivity of wadsleyite at high temperatures and high pressures. Earth Planet Sci Lett 287:277–283. doi:10.1016/j.epsl.2009.08.012

Dai L, Karato S (2014a) High and highly anisotropic electrical conductivity of the asthenosphere due to hydrogen diffusion in olivine. Earth Planet Sci Lett 408:79–86. doi:10.1016/j.eps1.2014.10.003

Dai L, Karato S-I (2014b) The effect of pressure on the electrical conductivity of olivine under the hydrogen-rich conditions. Phys Earth Planet Inter 232:51–56

Dai L, Karato S-I (2014c) Influence of oxygen fugacity on the electrical conductivity of hydrous olivine: implications for the mechanism of conduction. Phys Earth Planet Inter 232:57–60

Demouchy S (2010a) Diffusion of hydrogen in olivine grain boundaries and implications for the survival of water-rich zones in the Earth's mantle. Earth Planet Sci Lett 295:305–313. doi:10.1016/j.epsl.2010.04.019

Demouchy S (2010b) Hydrogen diffusion in spinel grain boundaries and consequences for chemical homogenization in hydrous peridotite. Contrib Mineral Petrol 160:887–898. doi:10.1007/s00410-010-0512-4

Demouchy S (2012) Erratum to "Diffusion of hydrogen in olivine grain boundaries and implications for the survival of water-rich zones in Earth's mantle" [Earth Planet. Sci. Lett. 295 (2010) 305–313] Earth Planet Sci Lett 351:355–355

Demouchy S, Bolfan-Casanova N (2016) Distribution and Transport of Hydrogen in the Lithospheric Mantle: a review. Lithos 240–243:402–425

Demouchy S, Mackwell S (2003) Water diffusion in synthetic iron-free forsterite. Phys Chem Miner 30:486–494. doi:10.1007/s00269-003-0342-2

Demouchy S, Mackwell S (2006) Mechanisms of hydrogen incorporation and diffusion in iron-bearing olivine. Phys Chem Miner 33:347–355. doi:10.1007/s00269-006-0081-2

Du Frane WL, Tyburczy JA (2012) Deuterium-hydrogen exchange in olivine: implications for point defects and electrical conductivity. Geochem Geophys Geosyst. doi:10.1029/2011gc003895

Duba A (1976) Are laboratory electrical conductivity data relevant to the Earth? Acta Geodaet Geophys et Montanist Acad Sci Hung 11:485–496

Duba A, Constable S (1993) The electrical-conductivity of lherzolite. J Geophys Res Solid Earth 98:11885–11899

Duba A, Nicholls IA (1973) Influence of oxidation state on electrical conductivity of olivine. Earth Planet Sci Lett 18:59–64

Farver JR (2010) Oxygen and hydrogen diffusion in minerals. In: Zhang YX, Cherniak DJ (eds) Diffusion in minerals and melts, vol 72. Reviews in mineralogy and geochemistry. Mineralogical Society of America, Chantilly, VA 20151-1110, United States, pp 447–507. doi:10.2138/rmg.2010.72.10

Farver JR, Yund RA, Rubie DC (1994) Magnesium grain-boundary diffusion in forsterite aggregates at 1000–1300 C and 0.1 MPa to 10 GPa. J Geophys Res Solid Earth 99:19809–19819. doi:10.1029/94jb01250

Ferot A, Bolfan-Casanova N (2012) Water storage capacity in olivine and pyroxene to 14 GPa: implications for the water content of the Earth's upper mantle and nature of seismic discontinuities. Earth Planet Sci Lett 349:218–230. doi:10.1016/j.epsl.2012.06.022

Fullea J, Muller MR, Jones AG (2011) Electrical conductivity of continental lithospheric mantle from integrated geophysical and

petrological modeling: application to the Kaapvaal Craton and Rehoboth Terrane, southern Africa. J Geophys Res Solid Earth. doi:10.1029/2011jb008544

Fyfe WS (1970) Lattice energies, phase transformations and volatiles in the mantle. Phys Earth Planet Inter 3:196–200

Gardes E, Gaillard F, Tarits P (2015) Toward a unified olivine electrical conductivity law. Geochem Geophys Geosyst. doi:10.1002/2014GC005496

Grant KJ, Kohn SC, Brooker RA (2007) The partitioning of water between olivine, orthopyroxene and melt synthesised in the system albite-forsterite-H(2)O. Earth Planet Sci Lett 260:227–241. doi:10.1016/j.epsl.2007.05.032

Green DH (1973) Experimental melting studies on a model upper mantle composition at high-pressure under water-saturated and water-undersaturated conditions. Earth Planet Sci Lett 19:37–53. doi:10.1016/0012-821x(73)90176-3

Green DH, Hibberson WO, Kovacs I, Rosenthal A (2010) Water and its influence on the lithosphere-asthenosphere boundary. Nature 467:448–451

Green DH, Hibberson WO, Kovacs I, Rosenthal A (2011) Water and its influence on the lithosphere-asthenosphere boundary. Nature 472:504

Green DH, Hibberson WO, Rosenthal A, Kovacs I, Yaxley GM, Falloon TJ, Brink F (2014) Experimental study of the influence of water on melting and phase assemblages in the upper mantle. J Petrol 55:2067–2096. doi:10.1093/petrology/egu050

Hilchie L, Fedortchouk Y, Matveev S, Kopylova MG (2014) The origin of high hydrogen content in kimberlitic olivine: evidence from hydroxyl zonation in olivine from kimberlites and mantle xenoliths. Lithos 202:429–441. doi:10.1016/j.lithos.2014.06.010

Hilt O, Siebbeles LDA (1998) Time and frequency dependent charge carrier mobility on one-dimensional chains with energetic disorder for polaron and Miller-Abrahams type hopping. Chem Phys 229:257–263. doi:10.1016/s0301-0104(98)00037-8

Hiraga T, Kohlstedt DL (2007) Equilibrium interface segregation in the diopside-forsterite system I: analytical techniques, thermodynamics, and segregation characteristics. Geochim Cosmochim Acta 71:1266–1280. doi:10.1016/j.gca.2006.11.019

Hiraga T, Kohlstedt DL (2009) Systematic distribution of incompatible elements in mantle peridotite: importance of intra- and inter-granular melt-like components. Contrib Mineral Petrol 158:149–167. doi:10.1007/s00410-009-0375-8

Hirschmann M, Kohlstedt DL (2012a) Water in Earth's mantle. Phys Today 65:40–45

Hirschmann MM, Kohlstedt D (2012b) Water in Earth's mantle. Phys Today 65:40–45

Hirth G (2006) Geophysics—protons lead the charge. Nature 443:927–928. doi:10.1038/nature05208

Hirth G, Kohlstedt DL (1995) Experimental constraints on the dynamics of the partially molten upper-mantle 2: deformation in the dislocation creep regime. J Geophys Res Solid Earth 100:15441–15449. doi:10.1029/95jb01292

Hirth G, Kohlstedt DL (1996) Water in the oceanic upper mantle: implications for rheology, melt extraction and the evolution of the lithosphere. Earth Planet Sci Lett 144:93–108. doi:10.1016/0012-821x(96)00154-9

Hirth G, Kohlstedt D (2003) Rheology of the Upper Mantle and the mantle wedge: a view from the experimentalists. In: Inside the subduction factory, vol 138. Geophysical monograph. American Geophysical Union, Washington, pp 83–105

Hoffman RE, Turnbull D (1951) Lattice and grain boundary self-diffusion in silver. J Appl Phys 22:634–639. doi:10.1063/1.1700021

Huang XG, Xu YS, Karato S-I (2005) Water content in the transition zone from electrical conductivity of wadsleyite and ringwoodite. Nature 434:746–749. doi:10.1038/nature03426

Ingrin J, Blanchard M (2006) Diffusion of hydrogen in minerals. Water in Nominally Anhydrous Minerals 62:291–320. doi:10.2138/rmg.2006.62.13

Jones AG (2014a) Compensation of the Meyer-Neldel compensation law for H diffusion in minerals. Geochem Geophys Geosyst 15:1–16. doi:10.1002/2014GC005261

Jones AG (2014b) Reconciling different equations for proton conduction using the Meyer-Neldel compensation rule. Geochem Geophys Geosyst 15:337–349. doi:10.1002/2013GC004911

Jones AG, Evans RL, Eaton DW (2009) Velocity-conductivity relationships for mantle mineral assemblages in Archean cratonic lithosphere based on a review of laboratory data and Hashin-Shtrikman extremal bounds. Lithos 109:131–143. doi:10.1016/j.lithos.2008.10.014

Jones AG, Fullea J, Evans RL, Muller MR (2012) Water in cratonic lithosphere: calibrating laboratory-determined models of electrical conductivity of mantle minerals using geophysical and petrological observations. Geochem Geophys Geosyst. doi:10.1029/2012gc004055

Jung H, Karato S-I (2001a) Effects of water on dynamically recrystallized grain-size of olivine. J Struct Geol 23:1337–1344. doi:10.1016/s0191-8141(01)00005-0

Jung H, Karato S-I (2001b) Water-induced fabric transitions in olivine. cience 293:1460–1463

Karato S-I (1990) The role of hydrogen in the electrical-conductivity of the upper mantle. Nature 347:272–273. doi:10.1038/347272a0

Karato S-I (2006) Remote sensing of hydrogen in Earth's mantle. In: Keppler H, Smyth JR (eds) Water in Nominally Anhydrous Minerals, vol 62. Reviews in mineralogy and geochemistry. pp 343–375. doi:10.2138/rmg.2006.62.15

Karato S-I (2011) Water distribution across the mantle transition zone and its implications for global material circulation. Earth Planet Sci Lett 301:413–423. doi:10.1016/j.epsl.2010.11.038

Karato S-I (2013) Theory of isotope diffusion in a material with multiple species and its implications for hydrogen-enhanced electrical conductivity in olivine. Phys Earth Planet Inter 219:49–54

Karato S-I (2015) Some notes on hydrogen-related point defects and their role in the isotope exchange and electrical conductivity in olivine. Phys Earth Planet Inter 248:94–98

Karato S-I, Dai L (2009) Comments on "Electrical conductivity of wadsleyite as a function of temperature and water content" by Manthilake et al. Phys Earth Planet Inter 174:19–21. doi:10.1016/j.pepi.2009.01.011

Karato S-I, Wang DJ (2013) Electrical conductivity of minerals and rocks. Wiley, Hoboken

Karato S-I, Wu P (1993) Rheology of the upper mantle: a synthesis. Science 260:771–778

Katayama I, Korenaga J (2011) Is the African cratonic lithosphere wet or dry? In: Beccaluva L, Bianchini G, Wilson M (eds) Volcanism and Evolution of the African Lithosphere, vol 478. Geological Society of America Special Papers. pp 249-256. doi:10.1130/2011.2478(13)

Kohlstedt DL, Mackwell SJ (1998) Diffusion of hydrogen and intrinsic point defects in olivine. Z Phys Chemie-Int J Res Phys Chem Chem Phys 207:147–162

Kohlstedt DL, Mackwell SJ (1999) Solubility and diffusion of 'water' in silicate minerals. In: Microscopic properties and processes in minerals, vol 543. Nato advanced science institutes series, series C, mathematical and physical sciences. pp 539–559

Kovacs I, Hermann J, O'Neill HSC, Gerald JF, Sambridge M, Horvath G (2008) Quantitative absorbance spectroscopy with unpolarized light: part II. Experimental evaluation and development of a protocol for quantitative analysis of mineral IR spectra. Am Miner 93:765–778. doi:10.2138/am.2008.2656

Kovacs I, O'Neill HSC, Hermann J, Hauri EH (2010) Site-specific infrared O-H absorption coefficients for water substitution into olivine. Am Miner 95:292–299. doi:10.2138/am.2010.3313

Kovacs I, Green DH, Rosenthal A, Hermann J, O'Neill HS, Hibberson WO, Udvardi B (2012) An experimental study of water in nominally anhydrous minerals in the upper mantle near the water-saturated solidus. J Petrol 53:2067–2093. doi:10.1093/petrology/egs044

Libowitzky E, Rossman GR (1996) Principles of quantitative absorbance measurements in anisotropic crystals. Phys Chem Miner 23:319–327

Mackwell SJ, Kohlstedt DL (1990) Diffusion of hydrogen in olivine—implications for water in the mantle. J Geophys Res Solid Earth Planets 95:5079–5088. doi:10.1029/JB095iB04p05079

Manthilake M, Matsuzaki T, Yoshino T, Yamashita S, Ito E, Katsura T (2009) Electrical conductivity of wadsleyite as a function of temperature and water content. Phys Earth Planet Inter 174:10–18. doi:10.1016/j.pepi.2008.06.001

Martin RF, Donnay G (1972) Hydroxyl in the mantle. Am Miner 57:554–570

Mei S, Kohlstedt DL (2000a) Influence of water on plastic deformation of olivine aggregates 1. Diffusion creep regime. J Geophys Res Solid Earth 105:21457–21469. doi:10.1029/2000jb900179

Mei S, Kohlstedt DL (2000b) Influence of water on plastic deformation of olivine aggregates 2. Dislocation creep regime. J Geophys Res Solid Earth 105:21471–21481. doi:10.1029/2000jb900180

Michael PJ (1988) The concentration, behaviour and storage of H2O in the sub-oceanic upper mantle: implications for mantle metasomatism. Geochim Cosmochim Acta 52:555–566

Murch GE (1983) The exact Nernst–Einstein equations and the interpretation of cross phenomenological coefficients in unary, binary, and ambipolar systems. Radiat Eff Defects Solids 73:299–305. doi:10.1080/00337578308220688

Naif S, Key K, Constable S, Evans RL (2013) Melt-rich channel observed at the lithosphere-asthenosphere boundary. Nature 495:356–359. doi:10.1038/nature11939

Ohuchi T et al (2015) In situ observation of crystallographic preferred orientation of deforming olivine at high pressure and high temperature. Phys Earth Planet Inter 243:1–21. doi:10.1016/j.pepi.2015.04.004

Padrón-Navarta JA, Hermann J, O'Neill HSC (2014) Site-specific hydrogen diffusion rates in forsterite. Earth Planet Sci Lett 392:100–112. doi:10.1016/j.epsl.2014.01.055

Peslier AH, Woodland AB, Bell DR, Lazarov M (2010) Olivine water contents in the continental lithosphere and the longevity of cratons. Nature 467:78–81. doi:10.1038/nature09317

Peslier AH, Bizimis M, Matney M (2015) Water disequilibrium in olivines from Hawaiian peridotites: recent metasomatism, H diffusion and magma ascent rates. Geochim Cosmochim Acta 154:98–117. doi:10.1016/j.gca.2015.01.030

Poe BT, Romano C, Nestola F, Smyth JR (2010) Electrical conductivity anisotropy of dry and hydrous olivine at 8 GPa. Phys Earth Planet Inter 181:103–111. doi:10.1016/j.pepi.2010.05.003

Pommier A (2014) Interpretation of magnetotelluric results using laboratory measurements. Surv Geophys 35:41–84. doi:10.1007/s10712-013-9226-2

Sambridge M, Gerald JF, Kovacs I, O'Neill HSC, Hermann J (2008) Quantitative absorbance spectroscopy with unpolarized light: part I. Physical and mathematical development. Am Miner 93:751–764

Schmadicke E, Gose J, Witt-Eickschen G, Bratz H (2013) Olivine from spinel peridotite xenoliths: Hydroxyl incorporation and mineral composition. Am Miner 98:1870–1880. doi:10.2138/am.2013.4440

Schmädicke E, Okrusch M, Rupprecht-Gutowski P, Will TM (2011) Garnet pyroxenite, eclogite and alkremite xenoliths from the off-craton Gibeon Kimberlite Field, Namibia: a window into the upper mantle of the Rehoboth Terrane. Precambrian Res 19:1–17. doi:10.1016/j.precamres.2011.07.010

Stalder R, Skogby H (2003) Hydrogen diffusion in natural and synthetic orthopyroxene. Phys Chem Miner 30:12–19. doi:10.1007/s00269-002-0285-z

Sundvall R, Skogby H, Stalder R (2009) Hydrogen diffusion in synthetic Fe-free diopside. Eur J Mineral 21:963–970. doi:10.1127/0935-1221/2009/0021-1971

ten Grotenhuis SM, Drury MR, Peach CJ, Spiers CJ (2004) Electrical properties of fine-grained olivine: evidence for grain boundary transport. J Geophys Res Solid Earth 109:9. doi:10.1029/2003JB002799

Waff HS (1974) Theoretical considerations of electrical-conductivity in a partially molten mantle and implications for geothermometry. J Geophys Res 79:4003–4010

Walker AM, Hermann J, Berry AJ, O'Neill HS (2007) Three water sites in upper mantle olivine and the role of titanium in the water weakening mechanism. J Geophys Res Solid Earth. doi:10.1029/2006jb004620

Wang Q (2010) A review of water contents and ductile deformation mechanisms of olivine Implications for the lithosphere-asthenosphere boundary of continents. Lithos 120:30–41. doi:10.1016/j.lithos.2010.05.010

Wang DJ, Mookherjee M, Xu YS, Karato S-I (2006) The effect of water on the electrical conductivity of olivine. Nature 443:977–980

Wang DJ, Li HP, Yi L, Shi BP (2008) The electrical conductivity of upper-mantle rocks: water content in the upper mantle. Phys Chem Miner 35:157–162. doi:10.1007/s00269-007-0207-1

Watson EB, Baxter EF (2007) Diffusion in solid-earth systems. Earth Planet Sci Lett 253:307–327. doi:10.1016/j.epsl.2006.11.015

Withers AC (2013) On the use of unpolarized infrared spectroscopy for quantitative analysis of absorbing species in birefringent crystals. Am Miner 98:689–697. doi:10.2138/am.2013.4316

Yang XZ (2012) Orientation-related electrical conductivity of hydrous olivine, clinopyroxene and plagioclase and implications for the structure of the lower continental crust and uppermost mantle. Earth Planet Sci Lett 317:241–250. doi:10.1016/j.epsl.2011.11.011

Yang XZ, Keppler H, McCammon C, Ni HW, Xia QK, Fan QC (2011) Effect of water on the electrical conductivity of lower crustal clinopyroxene. J Geophys Res Solid Earth. doi:10.1029/2010jb008010

Yang XZ, Keppler H, McCammon C, Ni HW (2012) Electrical conductivity of orthopyroxene and plagioclase in the lower crust. Contrib Mineral Petrol 163:33–48. doi:10.1007/s00410-011-0657-9

Yoshino T (2010) Laboratory electrical conductivity measurement of mantle minerals. Surv Geophys 31:163–206. doi:10.1007/s10712-009-9084-0

Yoshino T, Katsura T (2012) Re-evaluation of electrical conductivity of anhydrous and hydrous wadsleyite. Earth Planet Sci Lett 337:56–67. doi:10.1016/j.epsl.2012.05.023

Yoshino T, Katsura I (2013) Electrical conductivity of mantle minerals: role of water in conductivity anomalies. Ann Rev Earth Planet Sci 41:605–628. doi:10.1146/annurev-earth-050212-124022

Yoshino T, Matsuzaki T, Yamashita S, Katsura T (2006) Hydrous olivine unable to account for conductivity anomaly at the top of the asthenosphere. Nature 443:973–976. doi:10.1038/nature05223

Yoshino T, Manthilake G, Matsuzaki T, Katsura T (2008) Dry mantle transition zone inferred from the conductivity of wadsleyite and ringwoodite. Nature 451:326–329. doi:10.1038/nature06427

Yoshino T, Katsura T et al (2009a) Reply to Comments on "Electrical conductivity of wadsleyite as a function of temperature and water content" by Manthilake discussion. Phys Earth Planet Inter 174:22–23. doi:10.1016/j.pepi.2009.01.012

Yoshino T, Matsuzaki T, Shatskiy A, Katsura T (2009b) The effect of water on the electrical conductivity of olivine aggregates and its implications for the electrical structure of the upper mantle. Earth Planet Sci Lett 288:291–300. doi:10.1016/j.epsl.2009.09.032

Yurimoto H, Morioka M, Nagasawa H (1992) Oxygen self-diffusion along high diffusivity paths in forsterite. Geochem J 26:181–188

Zhang YX (2010) Diffusion in minerals and melts theoretical background. In: Diffusion in minerals and melts, vol 72. Reviews in mineralogy and geochemistry. pp 5–57. doi:10.2138/rmg.2010.72.2

Zhang YX, Cherniak DJ (2010) Diffusion in minerals and melts introduction. In: Diffusion in minerals and melts, vol 72. Reviews in mineralogy and geochemistry. pp 1–4. doi:10.2138/rmg.2010.72.1

Zhang BH, Shan SM (2015) Application of the cB Omega model to the calculation of diffusion parameters of Si in silicates. Geochem Geophys Geosyst 16:705–718. doi:10.1002/2014gc005551

Zhao ZF, Zheng YF (2007) Diffusion compensation for argon, hydrogen, lead, and strontium in minerals: empirical relationships to crystal chemistry. Am Miner 92:289–308. doi:10.2138/am.2007.2127

Proton conduction and hydrogen diffusion in olivine: An attempt to reconcile laboratory and field observations and implications for the role of grain boundary diffusion in enhancing conductivity

Supplementary Material

Alan G. Jones
Formerly Dublin Institute for Advanced Studies, 5 Merrion Square, Dublin 2, Ireland. Now at: Complete MT Solutions, 5345 McLean Crescent, Manotick, Ottawa, K4M 1E3, Canada.

Email: alan.jones.geophysics@gmail.com

Tel: +1-(613)-692-2854

1. Introduction

In this paper I examine not only electrical conductivity due to lattice diffusion of hydrogen, but also electrical conductivity due to grain boundary diffusion; taken together these are the bulk or effective diffusion of a multi-grain sample. Grain boundary diffusion is a well-known and well-established phenomenon in materials sciences, but is rather less appreciated in the geosciences. As discussed by Balluffi et al. (2005, Section 9.2, pp. 214-222), "*In a polycrystal containing a network of grain boundaries, atoms may migrate in both the grain interiors and the grain boundary slabs. They may jump into or out of boundaries during the time available, and spend various lengths of time jumping in the grains and along the boundaries*."

Karato (2013) stated that diffusion is dominated by slowest diffusing species whereas conductivity is dominated by fastest species – "*Consequently, the isotope diffusion coefficient is the harmonic average of diffusion coefficients of individual species and is dominated by the slowest diffusing species. In contrast, when electric current is carried by charged species, the concentrations of individual species do not change. Therefore, electrical conductivity is related to the arithmetic average of individual diffusion coefficients dominated by the fastest diffusing species*." I do not subscribe precisely to this view, as I consider different diffusing species to contribute in parallel both in diffusion and in conduction. I certainly subscribe to the view that the fastest diffusing process leads to the highest conductivity, and at laboratory conditions for polycrystalline samples I demonstrate that grain boundary diffusion dominates by orders of magnitude, whereas at lithospheric conditions for what we assume to be average grain sizes, then polaron conduction dominates unless there are well interconnected pathways of fine-grained wet material, e.g., veins of pyroxenes.

I focus on diffusion and conduction in olivine at a specific depth in the lithospheric mantle, and, as Jones et al. (2012), I take as my field-based standard the well-calibrated results at a depth of 100 km below the Jagersfontein (JAG) kimberlite field on the Kaapvaal Craton.

These are log(electrical conductivity) of -3.4 ±0.2 S/m, temperature of 740 ±50 °C, and water content (in the olivine) of 80 ±20 wt ppm (Bell calibration). I couple this with knowledge of the averaged grain size for the Kaapvaal Craton of 5-12 mm (Ave Lallemant et al. 1980, their Figure 7). I also consider the data from 100 km below the Gibeon (GIB) field on the Rehoboth terrane, where log(electrical conductivity) is -2.8 ±0.1 S/m, temperature is estimated at 850 ±50 °C, and water content in olivine is unknown, but was assumed to be also in the range 80 ±20 wt ppm in Jones et al. (2012). These olivine water contents have to be modified by assuming a partition model between grain boundary water and grain water, but as I show the partition model can be as large as 3:1 before measurable effects are seen.

1.1. FTIR spectra and water residence sites

There are a number of methods of identifying the presence of small amounts of water in the form of hydroxyls groups (OH) in mineral samples. These methods include Fourier transform infra-red (FTIR) spectroscopy, Raman spectroscopy, manometry, secondary ion mass spectrometry (SIMS), nuclear magnetic resonance (NMR), and elastic recoil detection analysis (ERDA) (e.g., Rossman (2006), ReMG). Among these techniques FTIR is preferred as it is the only one able to resolve site-specific information of the structural environment of the OH-groups. The use of FTIR to measure hydroxyl concentration (usually reported as ppm in weight of equivalent H_2O), however, relies on independent absolute measurements using standardless techniques such as manometry (Bell et al. 2003) or ERDA (Withers et al. 2012). Another disadvantage of FTIR measurements is that the absorbance related to the stretching of OH groups in most minerals is strongly dependent on the crystallographic orientation. Some approaches have been devised to circumvent this issue using polarized light (Asimow et al. 2006; Libowitzky and Rossman 1996; Withers 2013) or unpolarized light (Kovacs et al. 2008; Sambridge et al. 2008). It is important to note that FTIR is only sensitive to bonded hydrogen, and therefore the occurrence of weakly-bonded interstitial hydrogen cannot be detected. This fact may have serious implications (and limitations) for electrical conductivity measurements in the lab as it has been proposed that this kind of hydrogen is indeed the one controlling electrical conduction (Karato 2013), although that proposal was recently shown experimentally to be unsubstantiated (Du Frane and Tyburczy 2012).

Intensive experiments in the last decades have demonstrated the occurrence of different types of OH substitutions in olivine (see FTIR spectra in Figure 1, main text). As noted by e.g., Berry et al. (2005), Walker et al. (2007) and Kovacs et al. (2010), there are at least four different mechanisms for the incorporation of water in the olivine crystal structure. The most prevalent one in natural olivines from the Earth's upper mantle is associated with Ti^{4+} ([Ti]) (Berry et al. 2005); Ti-H is the defect where Ti has moved from the Si site to a Mg site, and is replaced by H, creating the 3571 cm^{-1} and 3525 cm^{-1} OH bands seen in FTIR spectroscopy (Peslier and Bizimis 2015). Two mechanisms are associated with silicon ([Si]) and magnesium ([Mg]) vacancies; Si-H corresponds to a substitution of H for Si in pure forsterite and is the slowest diffusing defect, and in FTIR spectra it is detected as the 3612 cm^{-1} band, whereas Mg-H corresponds to H replacing Mg, shows as a 3225 cm^{-1} OH band in FTIR olivine spectra and is the fastest diffusing defect(Peslier and Bizimis 2015). The fourth mechanism is associated with trivalent cation substitution ([triv]) of commonly Fe^{3+}, or

potentially also Al; The bands at 3356^{-1} and 3320–3325 cm^{-1} are linked to trivalent cations (Triv-H) (Peslier and Bizimis 2015). In addition to these point defects, hydrated planar defects, such as Ti-clinohumite lamellae, can also occur in olivine (e.g., Hermann et al. 2007; Mosenfelder et al. 2006b), but these are related to relatively low pressure (<3 GPa) cold (<750 °C) conditions.

These residence sites can be identified in the FTIR spectra, where absorption bands in the range of 3650-3450 cm^{-1} are termed Group I bands, and 3450-3200 cm^{-1} are termed Group II bands, according to the standard classification of Bai and Kohlstedt (1993), with a defined subset termed Group I-H represented by strong bands at 3525 and 3573 cm^{-1} (Mosenfelder et al. 2006a). These IR bands correspond to vibrational bond energies, and their interpretation and sensitivities to *P*, *T*, Ol composition, activity of SiO_2, and H_2O and O_2 fugacities (f_{H_2O} and f_{O_2}) are all strongly debated (see e.g., discussion and references in Gaetani et al. (2014)). Gaetani et al. (2014) recently demonstrated the dominance of f_{H_2O} on C_H^{Ol}, and that Fo content has no discernable effect on C_H^{Ol} between fosterite contents of 88.18 and 91.41.

For our purposes I refer to Berry et al. (2005) (cf. Figure 1, main text), who showed FTIR peaks in natural olivine at 3612 cm^{-1} for Si vacancy, 3572^{-1} and 3525 cm^{-1} for Ti point defects, 3410 cm^{-1} for Ti planar defect, 3355^{-1} and 3325 cm^{-1} for Fe^{3+} defect, and 3160 cm^{-1} for Mg vacancy, and to Kovacs et al. (2010) with [Mg] peaks at 3220 and 3160 cm^{-1}, [Ti] peaks at 3572 and 3525 cm^{-1}, trivalent peaks between 3300 and 3400 cm^{-1}, and [Si] peaks at 3613, 3593, 3579, 3567, 3551, 3535, 3478, 3450, and 3405 cm^{-1}. Note that the Group I-H bands relate to [Ti] defects, the dominant and most prevalent incorporation mechanism (Berry et al. 2005; Schmadicke et al. 2013).

1.2. Calibration of water in olivine

Determining the amount of "water" in a sample prior and subsequent to either diffusion or conduction experiments is absolutely crucial for ascertaining any water loss during the experiment. FTIR has been used in almost all experimental studies addressing the effect of water content on electrical conductivity, but not with consistent care. The reader is also referred to the excellent synopsis in the recent review by Demouchy and Bolfan-Casanova (2016). In principle, it is possible to accurately measure the water content if (1) the total absorbance (i.e. the sum of the absorbance along the three principal directions) and (2) the integral molar absorption coefficient are both known. The source of errors is coming from these two values.

Several absorption coefficients are currently available, some of them are non-mineral specific and frequency-dependent (Libowitzky and Rossman 1997; Paterson 1982), whereas others are mineral specific (Bell et al. 2003; Withers et al. 2012, for olivine and forsterite, respectively), or even site-specific for olivine (Kovacs et al. 2010). Unfortunately there is still no consensus on the most appropriate absorption coefficient for olivine. The water content obtained with different calibrations varies in a systematic way, and in principle, could be corrected from one calibration to another if sufficient information exists. For instance Bell et

al. (2003) suggested that their calibration differs by a factor of 2.3 and 3.5 from the one proposed by Paterson (1982) using polarized and unpolarized infrared light respectively. These FTIR estimates of water content were though subsequently challenged by Kovacs et al. (2010) who suggested, based on secondary ion mass spectrometry (SIMS), that wavenumber-dependent calibrations were inadequate and that water contents are likely three times greater than those from Bell calibration estimation. However, Withers et al. (2012) recently showed that elastic recoil detection analysis (ERDA) of H in synthetic olivine samples correlates with the SIMS results, and both were some two-thirds lower than Bell calibrated FTIR estimates. The Withers calibration (Withers et al. 2012) is becoming used more routinely within the diffusion community, but in this paper I attempt to normalize the conductivity measurements to a consistent Bell calibration (Bell et al. 2003), which represents the current standard.

The second source of errors is coming from the measurement of the total absorbance in anisotropic materials such as olivine. These have discussed in detailed by Libowitzky and Rossman (1996), Asimow et al. (2006), Sambridge et al. (2008), Kovacs et al. (2008), and recently by Withers (2013). The optimum approach is to measured oriented samples with polarized light (Libowitzky and Rossman 1996; Withers 2013), or to measure a certain amount on randomly oriented crystals with polarized light and then extract the synthetic spectra along principal directions (Asimow et al. 2006). Another approach, not as optimum but sufficient, is to multiply by a factor of three the average of a large number of randomly oriented unpolarized measurements. This later approach has been recently contested by Withers (2013) because it is only valid for certain thicknesses of the sample and for certain bands. However, when the optimal conditions are met, as discussed by Kovacs et al. (2008), unpolarized measurements on more than 10-15 randomly oriented crystals can results in satisfactory water content estimations. This has been also additionally proved empirically by Bolfan-Casanova et al. (2014, their Figure 1S).

Most of the experiments addressing the effect of water on the electrical conductivity of olivine (Dai and Karato 2014a; Dai and Karato 2014b; Dai and Karato 2014c; Wang et al. 2006; Yoshino et al. 2009; Yoshino et al. 2006) used unpolarized light on polycrystalline samples (i.e., an average of many randomly oriented crystals) and therefore, following Sambridge et al. (2008) and Kovacs et al. (2008), what they measured was 1/3 of the total absorbance. In addition, all of these studies used the Paterson calibration and (although not stated) an orientation factor of $\gamma=1/3$ because of their use of unpolarized light. This orientation factor was introduced by Paterson (1982) in his original formulation to account for the orientation of the OH dipole in uniaxial crystals. An orientation factor of 1/3, as used in the above-mentioned experimental studies, is only valid for an isotropic orientation of the OH dipole using either polarized or unpolarized IR light. This assumption is clearly not met for the high anisotropy of the OH dipole in olivine. Bell et al. (2003) suggested a correction factor of 3.5 of the Paterson calibration using unpolarized infrared light, but only in the case that the unpolarized measurement is performed with an incident beam exactly parallel to the [010] olivine direction. Due to the use of randomly oriented polycrystalline material in the electrical conductivity measurements, employing the factor of 3.5 suggested by Bell et al. (2003) is not generally justified, although the factor of 3 suggested by Ferot and Bolfan-

Casanova (2012) is argued as robust. In contrast to the source of uncertainty related to the absorption coefficient as noted above, the uncertainty in the calculation of the total absorbance assuming an isotropic OH dipole cannot be scaled to a simple factor. This results in non-systematic differences when compared to correctly derived polarized measurements.

Only Poe et al. (2010) and Yang (2012) performed polarized measurements on oriented crystals, and therefore their water constrains should be more accurate. Poe et al. (2010) used Bell calibration, but their spectra closely correspond to the ones calibrated by Withers et al. (2012), so a factor of 2/3 might be (easily) justified to yield correct water contents using the Withers et al. (2012) calibration. Bolfan-Casanova et al. (2014) have recently demonstrated that estimates of water content using Raman spectroscopy can also be calibrated against water content derived using FTIR spectra using Withers calibration. The advantage of Raman spectroscopy is that it can detect low orders of water content, ~40 ppm wt H_2O (Thomas et al. 2008), on very small samples due to the very high spatial resolution (~1 μm); such low water contents are possible with FTIR but larger samples are required because of the larger resolution of IR spectroscopy (~30 × 30 μm). Finally, Thomas et al. (2009) emphasize that mineral-specific calibrations must be adopted, based on their comparisons of water estimates from FTIR, SIMS, Raman spectroscopy, nuclear reaction analysis (NRA) and proton-proton scattering.

I recognize all of the issues detailed above related to IR spectra determination of the water content within the experimental samples. To be consistent throughout though, I adopt the Bell calibration (Bell et al. 2003), and I correct the Paterson calibration water contents of Karato's group and Yoshino's group by a factor of 3.5 given their use of unpolarized FTIR spectra. This is slightly higher than the factor of 3 suggested by Ferot and Bolfan-Casanova (2012), but well within the combined 30% error associated with IR spectra water estimates based on all of the various factors associated with the estimation (Demouchy and Bolfan-Casanova 2016).

I appreciate that the latest experimental results suggest that Bell calibration is likely a factor of 33% too high, so all values need to be multiplied by 2/3 to obtain the Withers calibration (Withers et al. 2012) to obtain the most likely estimate of water content in the samples. However, the main conclusions from my examination are unaffected by a factor of 2/3. For the Paterson calibrated olivine conductivity data, I plot the data twice, once at the original reported water content values (open symbols in figures), and the second time at the Bell corrected (x3.5) water content values (full symbols in figures); the true water content for each measurement lies within the two points, likely closer to the Bell calibration.

Note that the sample water contents given in Table 1 in Yoshino et al. (2009) are listed in both $H/10^6Si$ and in wt%, but the corresponding values are in disagreement by an order of magnitude. Jones (2014), Dai and Karato (2014b) and Gardes et al. (2015b) comment on this, pointing out that if the values in $H/10^6Si$ are the correct ones then the observations are more consistent with those of other laboratories. However, in their corrigendum Yoshino et al. (2014) state that the water content values in wt% are the correct ones; this makes their observations highly anomalous as I discuss in the main text.

1.3. Maximum amount of water at lithospheric conditions

The water storage capacity of nominally anhydrous minerals or rocks is "the concentration of water that can be sequestered in the mineral(s) without stabilizing a hydrous fluid or melt" (Hirschmann et al. 2005). Hirschmann et al. (2005) corrected the prior Paterson calibration results of Kohlstedt et al. (1996) for Bell calibration of Fo90 olivine by multiplying by a factor of 3, and fit the data to a curve for water content in olivine given by

$$\log\left(C_{H_2O}^{Ol}\right) = -1.194 + 2.263z^{0.128} \quad \text{(S1)}$$

where z is the depth (km) and $C_{H_2O}^{Ol}$ is in wt ppm. At depths of 50, 100, 150 and 200 km, formula **Error! Reference source not found.** yields maximum storage capacities in olivine of 345, 770, 1270 and 1840 wt ppm respectively.

I note that at lithospheric pressures of 2.5 GPa to 5 GPa (approx. 75-150 km depths), but not at higher pressures, the incorporation of Al into olivine (and pyroxene) may enhance water incorporation (Ferot and Bolfan-Casanova 2012); however the experiments of Ferot and Bolfan-Casanova (2012) were performed at lowermost lithospheric and sub-lithospheric temperatures (1175-1400 °C), so the general applicability of this observation over all lithospheric depths needs to be proven.

These maximum water storage capacities are far in excess of what is observed petrologically in olivine crystals that displayed little water loss during fast ascent (as exhibited through their flat core-to-rim hydrogen diffusion profiles) in xenoliths recovered from kimberlites (Peslier et al. 2008). Peslier et al. (2010) and Baptiste et al. (2012) undertook careful analyses of olivines found in peridotite xenoliths from multiple Kaapvaal Craton kimberlites, and observed maxima of up to 150 wt ppm (Bell calibration) at 4-5 GPa (120-150 km), with lower values at shallower and deeper depths, reducing to virtually dry (<15 wt ppm) at >6 GPa (180 km), consistent with the solubility formula given in Eq. (2) below for along the adiabat. A study by Katayama et al. (2011) on granular and sheared peridotites from Kimberley with P-T conditions of 4.1-5.4 GPa (approx. 120-150 km) and 950-1130 °C yielded water contents in olivine of up to 370 wt ppm H_2O (Bell calibration), with the bulk of the grains lying in the range 100-200 ppm and the grains from the sheared samples showing a prevalence for higher water contents (>100 ppm) and those from the granular samples a prevalence for lower water contents (<200 ppm) (see histogram in Fig. 5 in Katayama et al. 2011).

A similar recent study of xenoliths from the Udachnaya kimberlite on the Siberian Craton revealed, surprisingly given the Kaapvaal Craton results, virtually depth-independent water content in olivine of up to 323 ppm, with the largest values >300 ppm (Bell calibration) at the greatest depths of 6.5-7 GPa (195-210 km) (Doucet et al. 2014). Also surprisingly is that these olivine water contents exceeded those observed in ortho- and clinopyroxene, counter to prevailing water partition models that place more to far more water in the pyroxenes than in the olivine (e.g., Aubaud et al. 2004; Aubaud et al. 2007; Grant et al. 2007; Hirschmann et al. 2005), although the latest experiments suggest the two become equal at deep upper mantle depths (9 GPa, approx. 270 km) (Ferot and Bolfan-Casanova 2012). Note that these

heterogeneous water contents at all depths in the Udachnaya kimberlite are linked to metasomatism, i.e., peridotites that may have been near fluid/melts channels that have more water in them than ones that were less metasomatized, further away (A. Peslier, pers. comm., 2015).

For reference, at asthenospheric conditions below the base of the lithosphere in equilibrium with melt, Ardia et al. (2012) proposed a formula valid at 1450 °C for the pressure range 5-13 GPa to explain their laboratory observations of

$$C_{H_2O}^{Ol}(\text{ppm}) = 57.6(\pm 16) \times P(\text{GPa}) - 169(\pm 18) \ . \quad \text{(S2)}$$

For an asthenosphere at 150 km (5 GPa), the water storage capacity they determined was 57 ±26 wt ppm H_2O, and for thick lithosphere of 240 km (8 GPa) it increases to 254 ±60 ppm; these are for the Withers calibration, so for Bell calibration are 50% higher, i.e. 86 ppm at 150 km and 380 ppm at 250 km. A equation for the solubility of hydrogen in olivine along the adiabat is given by Ferot and Bolfan-Casanova (2012), and is

$$C_H^{olivine} = 45.828 \exp(0.0079z) \quad \text{(S3)}$$

where z is the depth (km), which yields solubilities of 68, 101, 150, and 223 at depths of 50, 100, 150 and 200 km.

2. Proton conduction in olivine

2.1. Conduction in olivine

2.1.1. Small polaron conduction and ionic conduction contributions

Small polaron conduction is enabled by electron holes hopping between ferrous (Fe^{2+}) and ferric (Fe^{3+}) iron, and is the dominant conduction process in dry olivine at shallow to middle lithospheric temperatures (<1000 °C). Ionic conduction dominates at higher temperatures (>1250 °C) as a consequence of the creation of cation magnesium vacancies $\left(V''_{Mg}\right)$. The physics of these two processes is described in detail in the excellent review paper of Yoshino (2010).

Grain size will be shown to be important for hydrogen diffusion. Very few studies have considered grain size effects for small polaron and ion vacancy conduction. Yang and Heidelbach (2012) demonstrated for clinopyroxene that at low temperatures (<1,000 °C), where small polaron conduction dominates, grain boundary conduction is unimportant. At high temperatures, where magnesium vacancy conduction dominates and for very fine grained zones (grains of size << 1 mm), ten Grotenhuis et al. (2004) proposed, in their study of grains of sizes 1.1 μm, 2.2 μm and 4.5 μm of synthetic forsterite, that grain boundary conduction becomes an important process and dominates over grain interior conduction. This result contradicts prior experiments of Roberts and Tyburczy (1991) who studied a far larger range of grain sizes (7-15, 35-45 and 75-180 μm) of natural olivines (San Carlos olivine,

SCO). The volume conductivity model of Yoshino et al. (2009) appears to also contradict the conclusion of ten Grotenhuis et al. (2004) for all reasonable grain sizes.

Recently, Jones et al. (2009), Fullea et al. (2011) and Pommier (2014) gave literature reviews of electrical conductivity of mantle minerals and presented Arrhenius parameters most consistent with laboratory observations. Here I follow Jones et al. (2009), from Hirsch et al. (1993), for its simpler formulation for small polaron conduction in olivine (the differences between Jones et al. (2009) and Fullea et al. (2011) are second-order), and Fullea et al. (2011), from Yoshino et al. (2009), for ionic magnesium vacancy conduction in olivine, viz.:

$$\sigma_{0sp}\left(T, X_{\mathrm{Fe}}\right) = \left(\frac{10^{6.54}}{T}\right) X_{\mathrm{Fe}}^{1.81} \quad \text{(S/m)}, \quad \Delta H_h = 1.35 \quad \text{(eV)} \quad , \tag{S4}$$

and

$$\sigma_{0i} = 10^{4.73} \quad \text{(S/m)}, \quad \Delta \mathrm{H}_i = 2.31 \quad \text{(eV)} \ , \tag{S5}$$

where X_{Fe} is the fractional iron content. For San Carlos olivine (SCO), which is the gold standard sample for conductivity and diffusion measurements, the Mg# is approximately 90-92.

Figure 2 (main text) shows a plot of small polaron conduction (thin black line labeled J2009) and magnesium vacancy conduction (thin blue line labeled F2001), and both summed together (thick red line), for dry olivine with Mg#=92.0 in the temperature range of the coldest cratonic mantle to the transition zone (400-1500 °C, where temperatures beyond the lithosphere-asthenosphere boundary, taken here as 1350 °C, are indicated by the purple hatched field). Note that small polaron conduction dominates at temperatures found in the upper and middle parts of the lithospheric mantle, whereas magnesium vacancy ion conduction dominates at temperatures found in the lowermost lithosphere and asthenosphere. The cross-over in dominance occurs at ~1200 °C, but for accurate computations magnesium vacancy effects must be considered at temperatures greater than ~900 °C, i.e., in the mid-lower lithosphere.

For this paper I am concerned with conductivity between 740 °C and 850 °C so I only need to consider small polaron conduction, σ_{0sp}, and not magnesium vacancy conduction (although it is included in the calculations for completeness). I choose that temperature range as those bound the likely temperatures at 100 km depth below the Jagersfontein (Kaapvaal Craton, South Africa) and Gibeon (Rehoboth Terrane, Namibia) kimberlite fields in Southern Africa; that depth was the basis of the studies of Jones et al. (2009) and Jones et al. (2013). From the Jones et al. (2009) formula given in Equation (2) (main text), the expected dry olivine conductivity at 100 km below Jagersfontein (JAG, T=740 °C, Mg# = 93.2, Jones et al. (2012)) is $\log_{10}(\sigma_h\left(T = 740, \mathrm{X}_{\mathrm{Fe}} = 0.068\right))$= -5.29, and below Gibeon (GIB, T=850 °C, Mg# = 91.75, Jones et al. (2012)) is $\log_{10}(\sigma_h\left(T = 850, \mathrm{X}_{\mathrm{Fe}} = 0.0825\right))$= -4.53. The Fullea et al. (2011) calculations yield $\log_{10}(\sigma)$ of -5.26 and -4.43 respectively (within 0.1 log unit), and the SEO3 model of Constable (2006) yields half an order of magnitude less conductive with $\log_{10}(\sigma)$ values of -5.87 and -5.12 respectively (QFM buffering, using the coefficients of

Myers and Eugster (1983) rather than those adopted by Constable (2006) that yield $\log_{10}(\sigma)$ of -5.81 and -5.00). As I will show below, regardless of which model is preferred these JAG and GIB small polaron conductivity values are far larger, by orders of magnitude, than proton conductivity predicted from lattice diffusion alone for the fastest diffusion rate of the hydrogen residence sites in the lattice (Du Frane and Tyburczy 2012) for 80 wt ppm water (dashed thin magenta line in Figure 2, main text, labeled DT2012).

2.2. Laboratory conductivity measurements of proton conduction in olivine

The first sets of experiments used Paterson calibration (Paterson 1982) to determine water content, whereas most of the later ones mostly used Bell calibration (Bell et al. 2003); see Table 1 (main text) for water contents (in wt ppm H_2O) of the samples and the water calibration used (i.e., whether Paterson or Bell) by the experimentalists. In order to compare these results with each other as closely as possible, those water contents derived from Paterson calibration have been assigned water contents a factor of 3.5 higher, consistent with the comparison between the calibrations made by Bell et al. (2003) for non-polarized FTIR spectra. I recognize that 3.5 was appropriate for those samples that Bell et al. (2003) analyzed, and that the actual correction factor may lie anywhere in the range of 2-4.

Recently, Gardes et al. (2015b) attempted to reconcile the disparate laboratory observations, and achieved an acceptable fit to all of the data through allowing very wide ranges of uncertainty on the water contents of most of the data. These uncertainties were a combination of random errors, generated through the imprecision of the measurements themselves, and bias errors generated through the inaccuracies associated with using an inappropriate estimation of the water content in the samples (unpolarized Paterson calibrations) – the latter gave rise to assumed bias errors from unity to x3.5. The authors concluded, based on the quality of fit they could obtain, that the Yoshino/Poe formalism for proton conduction (i.e., with $r=1$ and $\alpha \neq 0$) was the appropriate one to adopt.

The best fit model obtained by the authors for isotropic conductivity (listed in their Table 1 and plotted in Figure 2 (main text), dotted purple line, and Figure 3 (main text), blue dashed line) is with an activation energy (ΔH_{0p}) value that was the same as that obtained by Yoshino et al. (2009), i.e. 0.92 ± 0.07 eV cf. 0.92 ± 0.04 eV, and with an activation energy water dependence also virtually within error of that of Yoshino et al. (2009), i.e. α of 0.22 ± 0.05 eV/(wt%)$^{1/3}$ cf. 0.16 ± 0.02 eV/(wt%)$^{1/3}$, whereas the pre-exponent value is almost an order of magnitude more conducting, i.e. $\log_{10}(\sigma_0)$ of 2.75 ± 0.45 S/m cf. 1.9 ± 0.44 S/m (see Table 4 (main text) for all experimental models). (Note: the proton conduction model values for Gardes et al. (2015b) have been converted into eV from kJ/mol and water contents to wt% from wt ppm as recorded in their paper.) The full Gardes et al. (2015b) model, including the effects of small polaron, magnesium vacancies and proton conduction, for a temperature of 740 °C is shown in Figure 2 (main text, labeled G2015, dotted purple line) and Figure 3 (main text, labeled G2015, blue dashed line). However, again the extrapolated shape of the model for realistic lithospheric water contents (i.e., <200 wt ppm) is entirely dictated by the form of the equation used to fit the data (see **Error! Reference source not found.**B, main

text). Note that the model comes reasonably close to the JAG and GIB field data values, to within an order of magnitude, but does not fit them (Figure 2, main text).

2.2.1. Criticisms of laboratory work

Those who conduct electrical conductivity studies of olivine in the laboratory are strongly arguing in the literature in defense of their own results and in opposition of those of others. Particularly Karato and Yoshino have exchanged a number of criticisms of each other's work related to sample preparation, laboratory procedures, sensitivity of the sensing equipment, conductivity measurements, pressure conditions, oxygen fugacity conditions, water content evaluation, etc. (Dai and Karato 2014b; Karato 2011; Karato and Dai 2009; Karato and Wang 2013; Yoshino 2010; Yoshino and Katsura 2013; Yoshino and Katsura 2009; Yoshino et al. 2008, Supplementary Information). Yang (2012) is highly critical of prior experiments, citing a number of issues particularly in the work of Yoshino et al. (2006) and of Poe et al. (2010), and Karato (2015) discusses the anomalous nature of the results of Poe et al. (2010).

Most recently, Gardes et al. (2015a) raised a number of criticisms of the recent paper of Dai and Karato (2014a), which attests to explain the high and highly anisotropic electrical conductivity of the asthenosphere in terms of hydrogen diffusion in olivine. The Dai and Karato (2014a) results are being seriously considered, and are in danger of becoming adopted, by a number of workers interpreting their field data (e.g., Sarafian et al. 2015; Yang et al. 2015). The response by Dai and Karato (2015) to Gardes et al. (2015a) is not compelling, casting aspersions on the work of all others including, in the context of this paper, that diffusion coefficients determined by laboratories have uncertainties of a factor the of order of ±2. As I will show below, a factor of 2 does not become even close to explaining the polycrystal laboratory observations or the field observations in the mid-lithospheric cratonic mantle; diffusion rates within olivine grains are far too slow by orders of magnitude.

Many of the critical arguments made by the above authors are beyond appreciation by those who simply wish to use the results for interpretation of magnetotelluric data and are not intimately involved in laboratory experiments. Falling into that category are the concerns raised by Poe et al. (2010) and Yang (2012) about the use of Ni/NiO buffering by both Wang et al. (2006) and Yoshino et al. (2006) in their low pressure experiments. However, clearly understandable is that the data of Yoshino et al. (2006) are suspect given that the conductivity measurements were made at a single low frequency (0.01 Hz) rather than at multiple frequencies to ensure that the full complex impedance spectrum is mapped over two arcs; the inner arc at higher frequencies yielding the sample resistance and the outer smaller arc at low frequencies being a consequence of electrode effects (Yang 2012). Yoshino considered this issue to introduce at most a 10% error (Yoshino et al. 2008, Supplementary Information), but there are a number of other issues related to the Yoshino et al. (2006) dataset, such as dehydration during the experimental runs, that warrant their exclusion from further analysis.

The data of Wang et al. (2008) on dunite must also be considered suspect, as no FTIR spectra are reported to have been obtained prior and subsequent to the experiment, so water loss cannot be determined.

Yang (2012) is quite critical of the experiments of Poe et al. (2010) on the H-rich olivine samples, concluding that the measurements were likely flawed by dehydration. Also, Poe et al. (2010) only measured FTIR spectra subsequent to their experiments, so again water loss during experiment could not be determined.

A general caution stated by Yoshino and Katsura (2009) is that hydrogen-doped samples can release water in experiments at temperatures exceeding 900 K, thus emphasizing the need for very careful assessment of water content, and the locations of the water, both prior and subsequent to the experiments. Dai and Karato (2014a) discuss this issue in their paper in which they report on their experiments up to 1373 K, and elaborate on the techniques they adopted to ameliorate the problem.

In conclusion, none of the laboratory experiments reported to date are without significant and substantial criticism and all must be viewed with caution. These differences attest to the complexity and difficulty in performing these experiments and the exquisite care and attention to detail that is required for all steps. It is though certainly not the case that the average of all of these experiments, as performed by Gardes et al. (2015b), has any robust meaning.

4. Diffusion-to-conduction: The Nernst-Einstein equation

The concept of using diffusion to determine conductivity, and more particularly vice-versa, has been utilized for half a century, typically using the simplest form of the Nernst-Einstein equation for non-interacting charge carriers in a unary system (Murch 1983) that relates diffusion to conduction (when the system is in thermal equilibrium (Hilt and Siebbeles 1998)) by:

$$\sigma_H = fD_H C_H q^2 / kT \tag{S6}$$

where

σ_H is the conductivity (in S/m),

f is a unitless correction correlation factor (related to the Haven ratio), usually taken as 0.5-1.0,

D_H is the diffusivity of the charge carrier (in m^2/s),

C_H is the concentration of the charge carrier ($1/m^3$),

q is the charge (Coulomb),

k is Boltzmann's constant (Joule/Kelvin), and

T is temperature (Kelvin).

Some have proposed generalized Nernst-Einstein relations that are more applicable for nonlinear transport coefficients (Weinert and Mason 1980) or for high defect concentration solids (McKee 1981).

Nernst (1888), studying solutions of electrolytes, introduced the equation that was later also associated with Einstein's work on Brownian motion. Interestingly, the relation between

diffusion and conductivity was observed and reported independently by Townsend (1900), following Maxwell's paper on kinetic energy (see brief historical review in Weinert and Mason 1980), so we should be using the name "Nernst-Townsend-Einstein" for the equation.

Exact application of the simplified Nernst-Einstein equation is considered to have had limited success. Early experiments demonstrated that the conductivity derived from diffusion employing the Nernst-Einstein equation overestimates the actual conductivity by factors of up to 2-3 (Borucka et al. 1957; Borucka et al. 1956; Yang 1957), which is in this case negligible given the range of diffusion rates. (As an interesting aside, in contrast the Stokes-Einstein equation, that relates diffusion to viscosity, was shown to hold from even the earliest experiments (Yang 1957).) This observation has been replicated by others (Agarwal et al. 2011; Engel and Tomozawa 1975; Guissani and Guillot 1994; Kashyap et al. 2011; Levesque et al. 2013; Schuster et al. 2008), sometimes with an underestimate of the conductivity (by 20%) rather than an overestimate (Gottlieb and Sollner 1968). This so-called "correlation coefficient" between the derived diffusion and measured diffusion (or derived conductivity and measured conductivity), related to the Haven ratio (Murch 1982), is usually taken to be between 0.5-1.0. The Nernst-Einstein equation was shown to be invalid when the charge carrier relaxes during time, demonstrating that the system must be in thermal equilibrium for valid application (Hilt and Siebbeles 1998).

Notwithstanding these arguments, there are a number of publications verifying the application of the simple Nernst-Einstein equation (to within 10%-20%), particularly in the Solid State Physics community (Levesque et al. 2013; Packer et al. 2006). The equation has been used to determine conductivities from diffusion rates (Bertolo et al. 2004; Jeon et al. 2012), and diffusion rates based on conductivities (Barati and Coley 2006; Lu 1997); often the latter is far easier to measure experimentally than the former. For conduction in dry olivine at high temperatures (1200-1400 °C), i.e., ionic diffusion of Mg^{2+} or Fe^{2+}, the Nernst-Einstein equation was shown to be valid by Misener (1974).

In our context of hydrogen diffusion and proton conduction, as discussed by Schuster et al. (2008) the Nernst-Einstein relation only applies exactly if proton conductivity (diffusion of protonic charge carriers) and proton diffusion are identical processes. Huang et al. (2005), repeated in Karato (2006), Tyburczy (2008) and Karato (2013), argued that although the most abundant site for hydrogen is as a natural defect $(2\mathrm{H})_{\mathrm{M}}^{X}$, corresponding to two protons trapped at a metal site (Kohlstedt et al. 1996; Kohlstedt and Mackwell 1998), electrical conductivity is governed of the concentration of free protons, which is lower than the total concentration of hydrogen. The defect reaction

$$(2\mathrm{H})_{\mathrm{M}}^{X} = (\mathrm{H})_{\mathrm{M}}' + H' \quad (1)$$

predicts the exponent $r=0.75$ on the water content (C_w) in the Arrhenius equation (Equation (2), main text), which is within error of the derived value of Wang et al. (2006) of 0.62 ±0.15, rather than $r=1$ as is required for full compliance with the Nernst-Einstein equation, as assumed in the form of the equation adopted by Yoshino's group and Poe's group and more recently by Gardes et al. (2015b). This suggestion, that the role of free protons dominates conductivity but is not measured in diffusion experiments thus negating application of the

Nernst-Einstein equation, was belied by the recent work of Du Frane and Tyburczy (2012) who estimated the number of free protons to be less than 10%.

References

Agarwal M, Singh M, Jabes BS, Chakravarty C (2011) Excess entropy scaling of transport properties in network-forming ionic melts (SiO2 and BeF2). J Chem Phys 134. doi:10.1063/1.3521488

Ardia P, Hirschmann MM, Withers AC, Tenner TJ (2012) H2O storage capacity of olivine at 5-8 GPa and consequences for dehydration partial melting of the upper mantle Earth and Planetary Science Letters 345:104-116 doi:10.1016/j.epsl.2012.05.038

Asimow PD, Stein LC, Mosenfelder JL, Rossman GR (2006) Quantitative polarized infrared analysis of trace OH in populations of randomly oriented mineral grains Am Miner 91:278-284 doi:10.2138/am.2006.1937

Aubaud C, Hauri EH, Hirschmann MM (2004) Hydrogen partition coefficients between nominally anhydrous minerals and basaltic melts. Geophysical Research Letters 31:1-4. doi:10.1029/2004gl021341

Aubaud C, Withers AC, Hirschmann MM, Guan YB, Leshin LA, Mackwell SJ, Bell DR (2007) Intercalibration of FTIR and SIMS for hydrogen measurements in glasses and nominally anhydrous minerals Am Miner 92:811-828 doi:10.2138/am.2007.2248

Ave Lallemant HG, Mercier JCC, Carter NL, Ross JV (1980) Rheology of the upper mantle - Inferences from peridotite xenoliths Tectonophysics 70:85-113 doi:10.1016/0040-1951(80)90022-0

Bai Q, Kohlstedt DL (1993) Effects of chemical environment on the solubility and incorporation mechanism for hydrogen in olivine Phys Chem Miner 19:460-471

Balluffi RW, Allen SM, Carter WC (2005) Kinetics of Materials. Wiley-Interscience, Hoboken

Baptiste V, Tommasi A, Demouchy S (2012) Deformation and hydration of the lithospheric mantle beneath the Kaapvaal craton, South Africa Lithos 149:31-50 doi:10.1016/j.lithos.2012.05.001

Barati M, Coley KS (2006) Electrical and electronic conductivity of CaO-SiO2-FeOx slags at various oxygen potentials: Part II. Mechanism and a model of electronic conduction Metallurgical and Materials Transactions B-Process Metallurgy and Materials Processing Science 37:51-60 doi:10.1007/s11663-006-0085-9

Bell DR, Rossman GR, Maldener J, Endisch D, Rauch F (2003) Hydroxide in olivine: A quantitative determination of the absolute amount and calibration of the IR spectrum. Journal of Geophysical Research-Solid Earth 108. doi:10.1029/2001jb000679

Berry AJ, Hermann J, O'Neill HSC, Foran GJ (2005) Fingerprinting the water site in mantle olivine Geology 33:869-872 doi:10.1130/g21759.1

Bertolo E, Kilner JA, Sahibzada M (2004) Oxygen diffusion in SrCe0.95Yb0.05O3-delta Journal of Solid State Electrochemistry 8:585-591 doi:10.1007/s10008-003-0487-4

Bolfan-Casanova N, Montagnac G, Reynard B (2014) Measurement of water contents in olivine using Raman spectroscopy Am Miner 99:149-156 doi:10.2138/am.2014.4444

Borucka AZ, Bockris JO, Kitchener JA (1957) Self-diffusion in molten sodium chloride - a test of the applicability of the Nernst-Einstein equation Proceedings of the Royal Society of London Series a-Mathematical and Physical Sciences 241:554-567 doi:10.1098/rspa.1957.0146

Borucka AZ, Bockris JOM, Kitchener JA (1956) Test of the applicability of the Nernst-Einstein equation to self-diffusion and conduction of ions in molten sodium chloride J Chem Phys 24:1282-1282 doi:10.1063/1.1742795

Constable S (2006) SEO3: A new model of olivine electrical conductivity Geophysical Journal International 166:435-437 doi:10.1111/j.1365-246X.2006.03041.x

Dai L, Karato S (2014a) High and highly anisotropic electrical conductivity of the asthenosphere due to hydrogen diffusion in olivine Earth and Planetary Science Letters 408:79-86 doi:10.1016/j.eps1.2014.10.003

Dai L, Karato S-I (2014b) The effect of pressure on the electrical conductivity of olivine under the hydrogen-rich conditions Physics of the Earth and Planetary Interiors 232:51-56

Dai L, Karato S-I (2014c) Influence of oxygen fugacity on the electrical conductivity of hydrous olivine: Implications for the mechanism of conduction Physics of the Earth and Planetary Interiors 232:57-60

Dai L, Karato S-I (2015) Reply to comment on "High and highly anisotropic electrical conductivity of the asthenosphere due to hydrogen diffusion in olivine" by Dai and Karato [Earth Planet. Sci. Lett. 408 (2014) 79–86] Earth and Planetary Science Letters 427:300-302 doi:10.1016/j.epsl.2015.06.042

Demouchy S, Bolfan-Casanova N (2016) Distribution and Transport of Hydrogen in the Lithospheric Mantle: A Review Lithos in press

Doucet LS, Peslier AH, Ionov DA, Brandon AD, Golovin AV, Goncharov AG, Ashchepkov IV (2014) High water contents in the Siberian cratonic mantle linked to metasomatism: An FTIR study of Udachnaya peridotite xenoliths Geochim Cosmochim Acta 137:159-187 doi:10.1016/j.gca.2014.04.011

Du Frane WL, Tyburczy JA (2012) Deuterium-hydrogen exchange in olivine: Implications for point defects and electrical conductivity. Geochem Geophys Geosyst 13. doi:10.1029/2011gc003895

Engel JR, Tomozawa M (1975) Nernst-Einstein relation in sodium silicate glass Journal of the American Ceramic Society 58:183-185 doi:10.1111/j.1151-2916.1975.tb11438.x

Ferot A, Bolfan-Casanova N (2012) Water storage capacity in olivine and pyroxene to 14 GPa: Implications for the water content of the Earth's upper mantle and nature of seismic discontinuities Earth and Planetary Science Letters 349:218-230 doi:10.1016/j.epsl.2012.06.022

Fullea J, Muller MR, Jones AG (2011) Electrical conductivity of continental lithospheric mantle from integrated geophysical and petrological modeling: Application to the Kaapvaal Craton and Rehoboth Terrane, southern Africa. Journal of Geophysical Research-Solid Earth 116. doi:10.1029/2011jb008544

Gaetani GA, O'Leary JA, Koga KT, Hauri EH, Rose-Koga EF, Monteleone BD (2014) Hydration of mantle olivine under variable water and oxygen fugacity conditions. Contrib Mineral Petrol 167. doi:10.1007/s00410-014-0965-y

Gardes E, Gaillard F, Tarits P (2015a) Comment to "High and highly anisotropic electrical conductivity of the asthenosphere due to hydrogen diffusion in olivine" by Dai and Karato [Earth Planet. Sci. Lett. 408 (2014) 79–86] Earth and Planetary Science Letters 427:296-299 doi:10.1016/j.epsl.2015.06.041

Gardes E, Gaillard F, Tarits P (2015b) Toward a unified olivine electrical conductivity law Geochemistry, Geophysics, Geosystems in press doi:10.1002/2014GC005496

Gottlieb MH, Sollner K (1968) Failure of Nernst-Einstein equation to correlate electrical resistances and rates of ionic self-exchange across certain fixed charge membranes Biophysical Journal 8:515-&

Grant K, Ingrin J, Lorand JP, Dumas P (2007) Water partitioning between mantle minerals from peridotite xenoliths Contrib Mineral Petrol 154:15-34 doi:10.1007/s00410-006-0177-1

Guissani Y, Guillot B (1994) Coexisting phases and criticality in NaCl by computer-simulation J Chem Phys 101:490-509 doi:10.1063/1.468160

Hermann J, Gerald JDF, Malaspina N, Berry AJ, Scambelluri M (2007) OH-bearing planar defects in olivine produced by the breakdown of Ti-rich humite minerals from Dabie Shan (China) Contrib Mineral Petrol 153:417-428 doi:10.1007/s00410-006-0155-7

Hilt O, Siebbeles LDA (1998) Time and frequency dependent charge carrier mobility on one-dimensional chains with energetic disorder for polaron and Miller-Abrahams type hopping Chemical Physics 229:257-263 doi:10.1016/s0301-0104(98)00037-8

Hirsch LM, Shankland TJ, Duba AG (1993) Electrical conduction and polaron mobility in Fe-bearing olivine Geophysical Journal International 114:36-44

Hirschmann MM, Aubaud C, Withers AC (2005) Storage capacity of H2O in nominally anhydrous minerals in the upper mantle Earth and Planetary Science Letters 236:167-181 doi:10.1016/j.epsl.2005.04.022

Huang XG, Xu YS, Karato S-I (2005) Water content in the transition zone from electrical conductivity of wadsleyite and ringwoodite Nature 434:746-749 doi:10.1038/nature03426

Jeon SY, Choi MB, Im HN, Hwang JH, Song SJ (2012) Oxygen ionic conductivity of La2NiO4+delta via interstitial oxygen defect J Phys Chem Solids 73:656-660 doi:10.1016/j.jpcs.2012.01.006

Jones AG (2014) Reconciling different equations for proton conduction using the Meyer-Neldel compensation rule Geochemistry, Geophysics, Geosystems 15:337-349 doi:10.1002/2013GC004911

Jones AG, Evans RL, Eaton DW (2009) Velocity-conductivity relationships for mantle mineral assemblages in Archean cratonic lithosphere based on a review of laboratory data and Hashin-Shtrikman extremal bounds. Lithos 109:131-143. doi:10.1016/j.lithos.2008.10.014

Jones AG, Fishwick S, Evans RL, Muller MR, Fullea J (2013) Velocity-conductivity relations for cratonic lithosphere and their application: Example of Southern Africa. Geochem Geophys Geosyst 14:806-827. doi:10.1002/ggge.20075, ISSN: 1525-2027

Jones AG, Fullea J, Evans RL, Muller MR (2012) Water in cratonic lithosphere: Calibrating laboratory-determined models of electrical conductivity of mantle minerals using geophysical and petrological observations. Geochem Geophys Geosyst 13. doi:10.1029/2012gc004055

Karato S-I (2006) Remote sensing of hydrogen in Earth's mantle. In: Keppler H, Smyth JR (eds) Water in Nominally Anhydrous Minerals, vol 62. Reviews in Mineralogy & Geochemistry. pp 343-375. doi:10.2138/rmg.2006.62.15

Karato S-I (2011) Water distribution across the mantle transition zone and its implications for global material circulation Earth and Planetary Science Letters 301:413-423 doi:10.1016/j.epsl.2010.11.038

Karato S-I (2013) Theory of isotope diffusion in a material with multiple species and its implications for hydrogen-enhanced electrical conductivity in olivine Physics of the Earth and Planetary Interiors 219:49-54

Karato S-I (2015) Some notes on hydrogen-related point defects and their role in the isotope exchange and electrical conductivity in olivine Physics of the Earth and Planetary Interiors

Karato S-I, Dai L (2009) Comments on "Electrical conductivity of wadsleyite as a function of temperature and water content" by Manthilake et al Physics of the Earth and Planetary Interiors 174:19-21 doi:10.1016/j.pepi.2009.01.011

Karato S-I, Wang DJ (2013) Electrical conductivity of minerals and rocks. Wiley-Blackwell,

Kashyap HK, Annapureddy HVR, Raineri FO, Margulis CJ (2011) How Is Charge Transport Different in Ionic Liquids and Electrolyte Solutions? Journal of Physical Chemistry B 115:13212-13221 doi:10.1021/jp204182c

Katayama I, Michibayashi K, Terao R, Ando JI, Komiya T (2011) Water content of the mantle xenoliths from Kimberley and implications for explaining textural variations in cratonic roots Geol J 46:173-182 doi:10.1002/gj.1216

Kohlstedt DL, Keppler H, Rubie DC (1996) Solubility of water in the alpha, beta and gamma phases of (Mg,Fe)(2)SiO4 Contrib Mineral Petrol 123:345-357 doi:10.1007/s004100050161

Kohlstedt DL, Mackwell SJ (1998) Diffusion of hydrogen and intrinsic point defects in olivine Z Phys Chemie-Int J Res Phys Chem Chem Phys 207:147-162

Kovacs I, Hermann J, O'Neill HSC, Gerald JF, Sambridge M, Horvath G (2008) Quantitative absorbance spectroscopy with unpolarized light: Part II. Experimental evaluation and development of a protocol for quantitative analysis of mineral IR spectra Am Miner 93:765-778 doi:10.2138/am.2008.2656

Kovacs I, O'Neill HSC, Hermann J, Hauri EH (2010) Site-specific infrared O-H absorption coefficients for water substitution into olivine Am Miner 95:292-299 doi:10.2138/am.2010.3313

Levesque M et al. (2013) Structure and dynamics in yttrium-based molten rare earth alkali fluorides. J Chem Phys 138. doi:10.1063/1.4802986

Libowitzky E, Rossman GR (1996) Principles of quantitative absorbance measurements in anisotropic crystals Phys Chem Miner 23:319-327

Libowitzky E, Rossman GR (1997) An IR absorption calibration for water in minerals Am Miner 82:1111-1115

Lu XY (1997) Application of the Nernst-Einstein equation to concrete Cement and Concrete Research 27:293-302 doi:10.1016/s0008-8846(96)00200-1

McKee RA (1981) A generalization of the Nernst-Einstein equation for self-diffusion in high defect concentration solids Solid State Ion 5:133-136 doi:10.1016/0167-2738(81)90210-1

Misener DJ (1974) Cationic diffusion in olivine to 1400 °C and 35 kbar. In: Hoffmann AW, Gilleti BJ, Yoder HS, Yund RA (eds) Geochemical Transport and Kinetics, vol 634. Carnegie Institution of Washington, Washington, DC, pp 117-129

Mosenfelder JL, Deligne NI, Asimow PD, Rossman GR (2006a) Hydrogen incorporation in olivine from 2-12 GPa Am Miner 91:285-294 doi:10.2138/am.2006.1943

Mosenfelder JL, Sharp TG, Asimow PD, Rossman GR (2006b) Hydrogen incorporation in natural mantle olivine vol 168. American Geophysical Union, Washington

Murch GE (1982) The Haven ratio in fast ionic conductors Solid State Ion 7:177-198 doi:10.1016/0167-2738(82)90050-9

Murch GE (1983) The exact Nernst-Einstein equations and the interpretation of cross phenomenological coefficients in unary, binary, and ambipolar systems Radiation Effects and Defects in Solids 73:299-305 doi:10.1080/00337578308220688

Myers J, Eugster HP (1983) The system Fe–Si–O: oxygen buffer calibrations to 1,500K Contrib Mineral Petrol 82:75-90

Nernst W (1888) Zur Kinetik der in Losung befindlichen Korper. Erste Abhandlung. Theorie der Diffusion Z Phys Chem 2:613–637

Packer RJ, Tsipis EV, Munnings CN, Kharton VV, Skinner SJ, Frade JR (2006) Diffusion and conductivity properties of cerium niobate Solid State Ion 177:2059-2064 doi:10.1016/j.ssi.2006.03.044

Paterson MS (1982) The determination of hydroxyl by infrared absorption in quartz, silicate glasses and similar materials Bulletin De Mineralogie 105:20-29

Peslier AH, Bizimis M (2015) Water in Hawaiian peridotite minerals: A case for a dry metasomatized oceanic mantle lithosphere Geochem Geophys Geosyst 16:1211-1232 doi:10.1002/2015gc005780

Peslier AH, Woodland AB, Bell DR, Lazarov M (2010) Olivine water contents in the continental lithosphere and the longevity of cratons Nature 467:78-81 doi:10.1038/nature09317

Peslier AH, Woodland AB, Wolff JA (2008) Fast kimberlite ascent rates estimated from hydrogen diffusion profiles in xenolithic mantle olivines from southern Africa Geochim Cosmochim Acta 72:2711-2722

Poe BT, Romano C, Nestola F, Smyth JR (2010) Electrical conductivity anisotropy of dry and hydrous olivine at 8 GPa Physics of the Earth and Planetary Interiors 181:103-111 doi:10.1016/j.pepi.2010.05.003

Pommier A (2014) Interpretation of magnetotelluric results using laboratory measurements Surveys in Geophysics 35:41-84 doi:10.1007/s10712-013-9226-2

Roberts JJ, Tyburczy JA (1991) Frequency-dependent electrical-properties of polycrystalline olivine compacts Journal of Geophysical Research-Solid Earth 96:16205-16222 doi:10.1029/91jb01574

Rossman GR (2006) Analytical methods for measuring water in nominally anhydrous minerals. In: Keppler H, Smyth JR (eds) Water in Nominally Anhydrous Minerals, vol 62. Reviews in Mineralogy & Geochemistry. pp 1-28. doi:10.2138/rmg.2006.62.1

Sambridge M, Gerald JF, Kovacs I, O'Neill HSC, Hermann J (2008) Quantitative absorbance spectroscopy with unpolarized light: Part I. Physical and mathematical development Am Miner 93:751-764

Sarafian E et al. (2015) The electrical structure of the central Pacific upper mantle constrained by the NoMelt experiment Geochem Geophys Geosyst 16:1115-1132 doi:10.1002/2014gc005709

Schmadicke E, Gose J, Witt-Eickschen G, Bratz H (2013) Olivine from spinel peridotite xenoliths: Hydroxyl incorporation and mineral composition Am Miner 98:1870-1880 doi:10.2138/am.2013.4440

Schuster M, Kreuer KD, Steininger H, Maier J (2008) Proton conductivity and diffusion study of molten phosphonic acid H3PO3 Solid State Ion 179:523-528 doi:10.1016/j.ssi.2008.03.030

ten Grotenhuis SM, Drury MR, Peach CJ, Spiers CJ (2004) Electrical properties of fine-grained olivine: Evidence for grain boundary transport. Journal of Geophysical Research-Solid Earth 109:9. doi:10.1029/2003JB002799

Thomas SM, Koch-Muller M, Reichart P, Rhede D, Thomas R, Wirth R, Matsyuk S (2009) IR calibrations for water determination in olivine, r-GeO2, and SiO2 polymorphs Phys Chem Miner 36:489-509 doi:10.1007/s00269-009-0295-1

Thomas SM, Thomas R, Davidson P, Reichart P, Koch-Muller M, Dollinger G (2008) Application of Raman spectroscopy to quantify trace water concentrations in glasses and garnets Am Miner 93:1550-1557 doi:10.2138/am.2008.2834

Townsend JS (1900) The diffusion of ions into gases Philosophical Transactions of the Royal Society of London Series a-Containing Papers of a Mathematical or Physical Character 193:129-158 doi:10.1098/rsta.1900.0004

Tyburczy JA (2008) Properties of Rocks and Minerals - The Electrical Conductivity of Rocks, Minerals, and the Earth. In: Price GD (ed) Mineral Physics, vol 2. Treatise on Geophysics Elsevier, pp 631-642

Walker AM, Hermann J, Berry AJ, O'Neill HS (2007) Three water sites in upper mantle olivine and the role of titanium in the water weakening mechanism. Journal of Geophysical Research-Solid Earth 112. doi:10.1029/2006jb004620

Wang DJ, Li HP, Yi L, Shi BP (2008) The electrical conductivity of upper-mantle rocks: water content in the upper mantle Phys Chem Miner 35:157-162 doi:10.1007/s00269-007-0207-1

Wang DJ, Mookherjee M, Xu YS, Karato S-I (2006) The effect of water on the electrical conductivity of olivine Nature 443:977-980

Weinert U, Mason EA (1980) Generalized Nernst-Einstein relations for non-linear transport-coefficients Physical Review A 21:681-690 doi:10.1103/PhysRevA.21.681

Withers AC (2013) On the use of unpolarized infrared spectroscopy for quantitative analysis of absorbing species in birefringent crystals Am Miner 98:689-697 doi:10.2138/am.2013.4316

Withers AC, Bureau H, Raepsaet C, Hirschmann MM (2012) Calibration of infrared spectroscopy by elastic recoil detection analysis of H in synthetic olivine Chemical Geology 334:92-98 doi:10.1016/j.chemgeo.2012.10.002

Yang B, Egbert GD, Kelbert A, Meqbel NM (2015) Three-dimensional electrical resistivity of the north-central USA from Earth Scope long period magnetotelluric data Earth and Planetary Science Letters 422:87-93 doi:10.1016/j.epsl.2015.04.006

Yang L (1957) Validity of Nernst-Einstein and Stokes-Einstein relationships in molten NaNO2 J Chem Phys 27:601-602 doi:10.1063/1.1743790

Yang XZ (2012) Orientation-related electrical conductivity of hydrous olivine, clinopyroxene and plagioclase and implications for the structure of the lower continental crust and uppermost mantle Earth and Planetary Science Letters 317:241-250 doi:10.1016/j.epsl.2011.11.011

Yang XZ, Heidelbach F (2012) Grain size effect on the electrical conductivity of clinopyroxene Contrib Mineral Petrol 163:939-947 doi:10.1007/s00410-011-0707-3

Yoshino T (2010) Laboratory electrical conductivity measurement of mantle minerals Surveys in Geophysics 31:163-206 doi:10.1007/s10712-009-9084-0

Yoshino T, Katsura I (2013) Electrical conductivity of mantle minerals: Role of water in conductivity anomalies Annual Reviews of Earth and Planetary Science 41:605-628 doi:10.1146/annurev-earth-050212-124022

Yoshino T, Katsura T (2009) Reply to Comments on "Electrical conductivity of wadsleyite as a function of temperature and water content" by Manthilake et al. Discussion Physics of the Earth and Planetary Interiors 174:22-23 doi:10.1016/j.pepi.2009.01.012

Yoshino T, Manthilake G, Matsuzaki T, Katsura T (2008) Dry mantle transition zone inferred from the conductivity of wadsleyite and ringwoodite Nature 451:326-329 doi:10.1038/nature06427

Yoshino T, Matsuzaki T, Shatskiy A, Katsura T (2009) The effect of water on the electrical conductivity of olivine aggregates and its implications for the electrical structure of the upper mantle Earth and Planetary Science Letters 288:291-300 doi:10.1016/j.epsl.2009.09.032

Yoshino T, Matsuzaki T, Shatzkiy A, Katsura T (2014) The effect of water on the electrical conductivity of olivine aggregates and its implications for the electrical structure in the upper mantle (vol 288, pg 291, 2009) Earth and Planetary Science Letters 391:135-136 doi:10.1016/j.epsl.2014.02.016

Yoshino T, Matsuzaki T, Yamashita S, Katsura T (2006) Hydrous olivine unable to account for conductivity anomaly at the top of the asthenosphere Nature 443:973-976 doi:10.1038/nature05223